Cellulose nanofibers to improve the mechanical and durability performance of self-healing Ultra-High Performance Concretes exposed to aggressive waters

Estefania Cuenca[1,*], Valentin Postolachi[1] and Liberato Ferrara[1]

ABSTRACT

The effects of including cellulose nanofibers (CNFs) in Ultra High Performance Concretes (UHPCs) have been studied in this paper in terms of recovery of both durability and mechanical properties because of the stimulated self-healing behavior. To this purpose, flexural tests on 4-point bending on 30 mm thin and 100 mm wide beam specimens have been carried out to evaluate the mechanical recovery due to self-healing, together with Double Edge Wedge Splitting tests that have been performed to identify the tensile stress crack-opening behavior. Moreover, water permeability and chloride diffusion tests have been performed to evaluate the recovery of durability properties on healed specimens subjected to extremely aggressive environments rich in chlorides and sulfates. Microstructural analysis has been also performed to confirm the enhancement on durability performance due to the presence of CNFs. The presence of CNFs has improved self-healing performance of UHPC since for the same crack width value and same healing period (1, 3 or 6 months) the specimens with CNFs reached higher crack sealing rates compared to those without nano-additions. As a matter of fact, the total sealing of the cracks over the 6 month investigated period was only observed on specimens with CNFs.

Keywords: Self-healing, crystalline admixtures, cellulose nanofibers, Ultra High Performance Fiber Reinforced Concrete.

[1] Department of Civil and Environmental Engineering, Politecnico di Milano, piazza Leonardo da Vinci 32, 20133, Milano Italy

* corresponding author, estefania.cuenca@polimi.it

1. INTRODUCTION

Construction industry represents 6% of the world Gross Domestic Product (GDP) [1]. With 10 billion tons produced and used yearly, concrete is the second largest used material worldwide (the first one is water), twice as much than the total of all other building materials, mainly because of its well-known versatility and advantages in the construction context. Nonetheless, reinforced concrete structures exposed to extremely aggressive environments need continuous

maintenance along their service life, primarily because of the sensitivity of the reinforcement, necessarily employed to temper the inherent weakness and brittleness of concrete in tension, to the corrosion induced by different environment born aggressive substances. For this reason, the durability of reinforced concrete structures has been and continues to be a topic of increasing interest in the scientific community and in the society since maintenance interventions are expensive and increase all along the service life of the reinforced concrete structures [2], [3]. In fact, yearly cost of corrosion reaches a 3.4% world GDP. Matthews [4] reported that 50% of repaired concrete structures failed once again, 25% of which in the first 5 years, 75% within 10 years and 95% within 25 years. To increase the service life of reinforced concrete structures exposed to aggressive environments the development, validation and widespread use of new and more durable materials such as Ultra High Performance Concretes (UHPC) is of the utmost importance and necessity. UHPC has a very compact matrix with an accessible porosity below 5% [5]. Moreover, the use of very low water/binder ratios (below 0.2), high amounts of binder (700-1000kg/m^3) and a very fine granular structure leads to a high durability in the uncracked state, an elevated compressive strength (120-150MPa) and direct tensile strength values in the range of 5-10MPa [6], [7], [8]. Nonetheless, due to these characteristics the unreinforced UHPC matrix results can be very brittle, also prone to internal microcracking due to high autogenous shrinkage. For this reason, the addition of fibers to UHPC is nowadays customary (in some cases the fiber reinforced composite is also denoted as Ultra High Performance Fiber Reinforced Concrete-UHPFRC) resulting into a signature tensile behavior, characterized by multiple cracking and strain hardening response, implying higher ductility and energy absorption capacity. Those characteristics are particularly interesting since reinforced structures are designed to work in cracked state over their service life. It is well-known that cracks allow the entrance of harmful substances such as chlorides and sulfates which endanger the durability of concrete [9] and the penetration of the aggressive agents is correlated with the opening of each single crack. In this context, while the capacity of UHPC to spread an otherwise localized damage into multiple tiny opened and closely spaced cracks is conducive to higher durability in the cracked state, self-healing techniques could bring additional benefits, enabling self-repairing of the cracks and, as a consequence, leading to improved durability and longer service life of concrete structures with less frequent need for repair and maintenance works [10], [11], [12]. The use of crystalline admixtures is nowadays a consolidated technology to stimulate the autogenous healing capacity of ordinary and even ultra-high performance concrete, which in the latter case relies on the aforesaid peculiar mix design composition [5], [13]. Crystalline admixtures are widely available on the market, often

"labeled as" permeability reducing admixtures. Their self-healing stimulating action is based on their high hydrophilicity, which leads them to react with water and cement hydration products as well, forming insoluble products and increasing the calcium silicate hydrates (C-S-H) in the matrix [14], [15], thus filling pores and cracks and reducing the overall permeability of cracked and uncracked concrete. As a matter of fact, the combination of self-healing techniques and UHPC can further benefit from the crack width control capacity provided by the fibers, the thinner the crack, the easier its healing [16], [14]. Through-crack reconstruction of matrix continuity as well as healing at the fiber-matrix bond level also can result into a stable holding of the mechanical performance of the material upon cracking/healing scenarios even in aggressive conditions [10], [17], [18].

In the last years, research has been carried out to promote the adoption of nanotechnology by the concrete construction industry [19], [20], [21]. The advantages of the use of nanomaterials in concrete are numerous due to the possibility to achieve higher compaction levels, reducing the porosity of the concrete matrix and its transport properties and hence improving the durability of the uncracked matrix. Other advantages are an enhanced corrosion resistance [22], self-curing ability [23], [24] and the enhancement of the durability in cracked state [5], [11]. Some of the most used nanomaterials are silica, titanium dioxide, nanoclays, carbon nanotubes, carbon nanofibers, alumina nanofibers and cellulose nanostructures [25], [10]. The latter are particularly interesting from a sustainability point of view. Cellulose-based materials combine the cellulose properties (high strength and stiffness and low weight) with the particular characteristics of nanomaterials, including high reactivity and high specific surface [26], [27], [28], [29], [30], [31]. As a matter of fact, some studies [32], [33] have highlighted a significant improvement of the mechanical properties of cementitious composites due to the presence of cellulose nanomaterials. Cao [34] observed a 30% increase in the flexural strength of cement pastes enriched with cellulose nanocrystals (CNCs) due to accelerated hydration reactions. Moreover, a slight increase in compressive strength was also observed mainly due to the high crystallinity index of CNCs and to the filling capacity acting at a pore level [35], [34], [36], [5], [16], [29], [31], [30], [37]. Further studies confirmed the aforesaid positive effects on mechanical performance also for cellulose nanofibers (CNFs) [28], [35], [38], [32], [25], [16]. In fact, CNFs act as nucleation sites enabling hydration of cement in early states due to their hydrophilic nature and highly reactive surface, which results into an increase of the amount of products which precipitate filling the pores, leading to a more compacted microstructure. The high absorption capacity of CNFs results especially interesting since they can act as water reservoirs that release water gradually when concretes are exposed to dry environments,

allowing continuous hydration which means a better self-healing of microcracks, similarly to what observed for natural vegetable fibers [39]. At the same time, they have a bridging effect on the microcracks controlling their propagation [27], [35], [38], [40].

Cuenca et al. [16] also studied the influence of CNCs and CNFs in UHPCs exposed to aggressive environments, in particular immersed in waters rich in chlorides and sulfates from a geothermal power plant. In all cases, the presence of nanomaterials was very positive, especially for the case of CNFs. The flexural strength for the specimens with CNFs was higher than for the other nanomaterials when specimens were cured both in moist room and immersed in geothermal water. Moreover, the autogenous and drying shrinkage was much lower in presence of CNFs. Self-healing was also improved in presence of CNFs since a 100% of crack sealing was reached after 6 months healing in both studied exposures, immersion in geothermal water and wet/dry cycles in the same aggressive water.

In order to further validate the aforesaid preliminary results, a comprehensive experimental campaign has been carried out in this work to analyze the mechanical and durability performance of self-healing UHPC exposed to aggressive waters rich in chlorides and sulfates, as a necessary step for a full scale validation of the aforesaid materials in a water basin built in a geothermal power plant in the framework of H2020 ReSHEALience project (GA 760824) for which continuous monitoring and validation is scheduled until 2025 [41], [42], [43]. Flexural tests on 4-point bending tests on 30 mm thin and 100 mm wide beam specimens have been carried out to evaluate the mechanical recovery due to self-healing, together with Double Edge Wedge Splitting tests have been performed to identify the tensile stress crack-opening behavior. Moreover, water permeability and chloride diffusion tests have been performed to evaluate the recovery of durability properties on healed specimens subjected to extremely aggressive environments rich in chlorides and sulfates, supported by microstructural analyses to assess the influence of cellulose nanomaterials.

2. EXPERIMENTAL PROGRAM

2.1. Materials and mix design

The mix design of the Ultra-High Performance Fiber Reinforced Concrete (UHPFRC) with cellulose nanofibers (CNFs) used in this research is shown in Table 1. The chemical composition of the employed cement CEM I 52.5R and slag are reported in Table 2 and in Figure 1 (a-d) the Scanning Electron Microscope (SEM) and Energy Dispersive X-ray (EDS) analysis of the employed cement and slag are showed. As fine aggregates, a crushed sand was employed whose particle size distribution is indicated in Table 3.

Table 1. Mix composition of the investigated UHPFRCC with CNFs (dosages in kg/m^3)

Constituents	**kg/m^3**
Cement CEM I 52.5R	600
Slag	500
Water	200
Steel fibers (l_f = 20 mm; d_f = 0.22 mm) Azichem Readymesh ®	120
Sand (0-2 mm)	982
Superplasticizer	33
Crystalline admixtures Penetron Admix ®	4.8
Cellulose nanofibers [0.15 % by cement mass]	0.9

Table 2. Chemical composition of the employed cement and slag.

(LOI: loss on ignition @1000°C).

Oxide (wt.%)	CaO	SiO_2	Al_2O_3	MgO	SO_3	Fe_2O_3	TiO_2	Mn_2O_3/ MnO	K_2O	Na_2O	Other	LOI
PC	59.7	19.5	4.9	3.3	3.4	3.5	0.2	0.1	0.8	0.2	0.4	2.5
BFS	39.2	38.9	10.2	6.4	1.3	0.4	0.6	0.3	0.5	0.8	0.3	1.2

Table 3. Particle size distribution of the employed crushed sand

Sieve diameter (mm)	**0.2**	**0.35**	**0.45**	**0.60**	**1.00**	**1.50**	**2.00**
Passing %	14.6	24.3	34.1	43.8	63.5	81.7	100

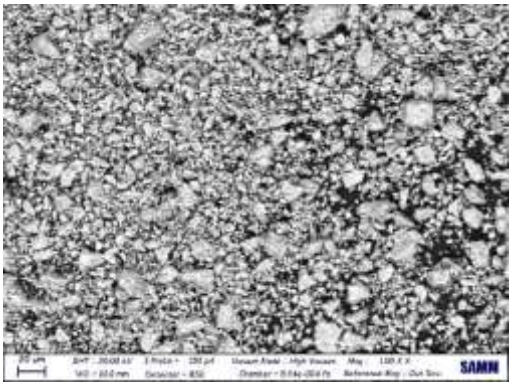

(a) SEM image of the employed cement

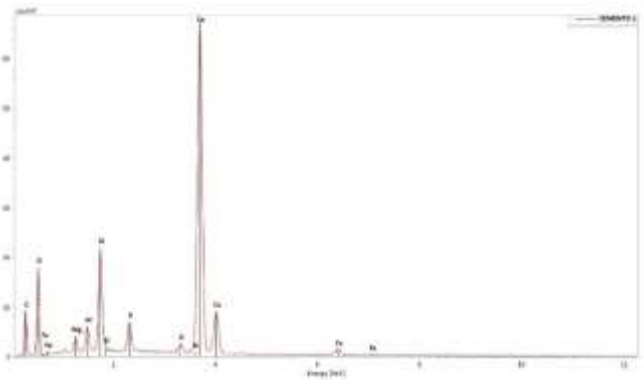

(b) EDS of the employed cement

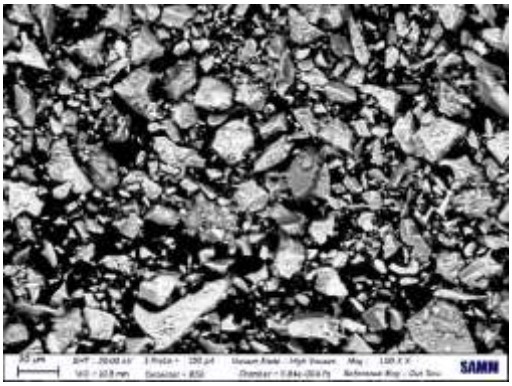

(c) SEM image of the employed slag

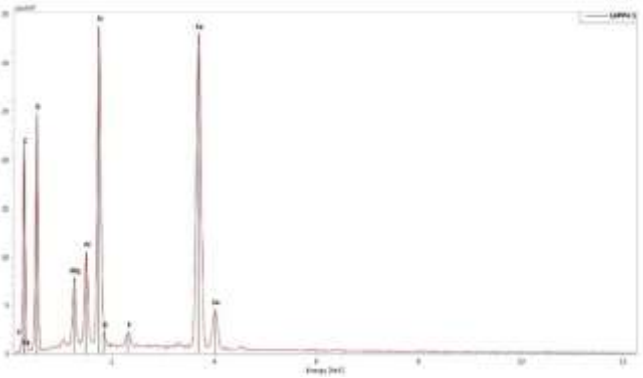

(d) EDS of the employed slag

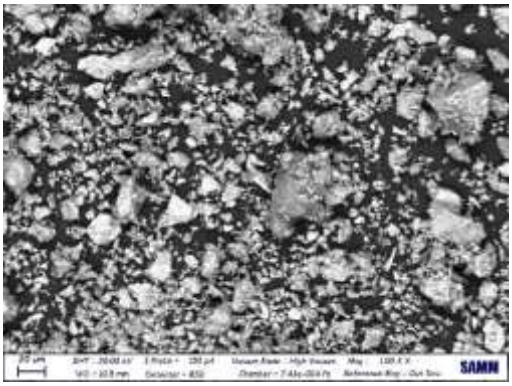

(e) SEM image of the employed crystalline admixtures

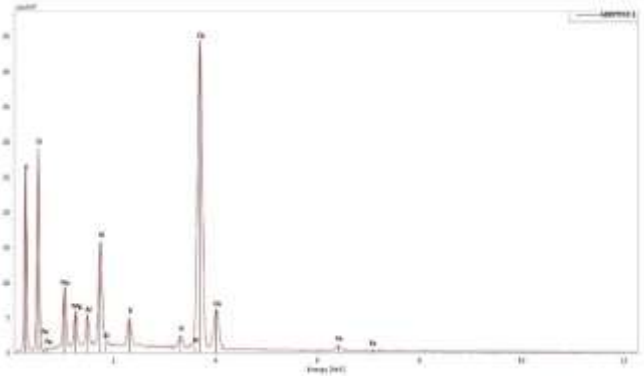

(f) EDS of the employed crystalline admixtures

Figure 1. SEM and EDS analysis of cement, slag and crystalline admixtures

Steel fibers (l_f = 20 mm; d_f = 0.22 mm) at volume fraction equal to 1.5% were added into the mix to guarantee the required strain-hardening tensile behavior [18]. Crystalline admixtures were added as promoters of the autogenous self-healing at 0.8% of cement weight. The morphological and chemical characteristics of the crystalline admixture were already described by Cuenca et al. [44], being it constituted by powder materials including Portland cement, quartz sand and other reactive proprietary chemicals [45]. In Figure 1 e-f the SEM and EDS

analysis of the employed crystalline admixtures are shown. The SEM image (Figure 1e) shows that the employed crystalline admixtures are characterized by particles of irregular shape, like cement and slag, ranging from 1 to 20μm and the EDS analysis shows that crystalline admixtures contain calcium, oxygen, silicon, magnesium, aluminum and potassium (Figure 1f). Aqueous suspension of cellulose nanofibers (CNFs), developed by the University of Maine has been used. CNFs are white and odorless, the nominal fiber width is 50nm with lengths of up to several hundred microns. Their specific surface is in the 31-33 m^2/g range. Figure 2a shows a SEM image of the employed CNFs whereas in Figure 2b the aspect is illustrated of the aqueous slurry of CNFs before being dispersed in water for mixing. A comprehensive characterization of the properties of CNFs as well as of the tailored mix-design protocol can be found in [25]. CNFs were added during the concrete mix but previously they were dispersed in water at a loading of 1.5% wt to facilitate their incorporation into a concrete with a low water/binder ratio.

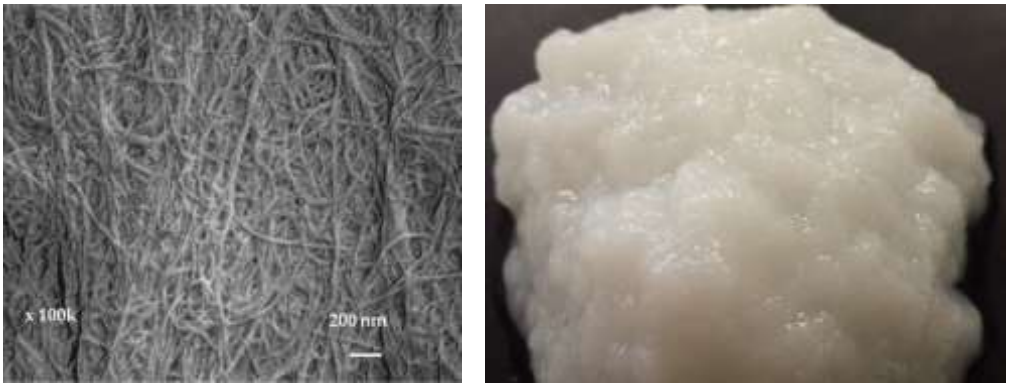

(a) (b)

Figure 2. (a) SEM image of the employed CNFs; (b) aqueous slurry of CNFs (courtesy of UMaine)

2.2. Preparation of specimens and tests methods

With the mix shown in Table 1, two slabs (1000x500x30mm), ten cubes (100x100x100mm), six prismatic specimens (100x100x500mm) and six cylinders (Ø100x300mm) were casted. The slabs were used to produce thin beams by further saw-cutting as detailed in the following. The cubes ($100x100x100mm^3$) were used to test compressive strength, whereas prismatic (deep beams $100x100x500mm^3$) and thin beams ($30x100x500mm^3$) were used to investigate the mechanical properties under flexural conditions. The cylinders were used for chlorides diffusion tests and water permeability tests, the last ones on disks obtained from the cylinders. Moreover, from the thin beams DEWS specimens were also obtained for indirect tensile tests.

The concrete pouring into the thin slab was particularly interesting since fibers are strongly oriented along the casting flow. In order to consider the fiber orientation into this study the casting procedure was specially designed. The casting started at one end of the slab and concrete flowed along the formwork until covering the entire surface of it. In this way, the upper layer of the concrete slide over the lower one, aligning the fibers with the direction of the concrete flow and stopping when it encounters the formwork edges (Figure 3). However, the area closer to the pouring point is a "turbulent" zone since the alignment is still not well developed. This fact was considered in the study when thin specimens were obtained from the slab.

All specimens were cured in moist room for 28 days at 20ºC and 95% RH. After curing, the slab was cut to obtain 20 thin beams (500x100x30mm), 10 specimens for each slab (Figure 3). Each single thin beam was identified with two numbers in order to know the exact position in the former slab. The first number to identify the former slab and the second number to know the position of the thin beam inside the slab.

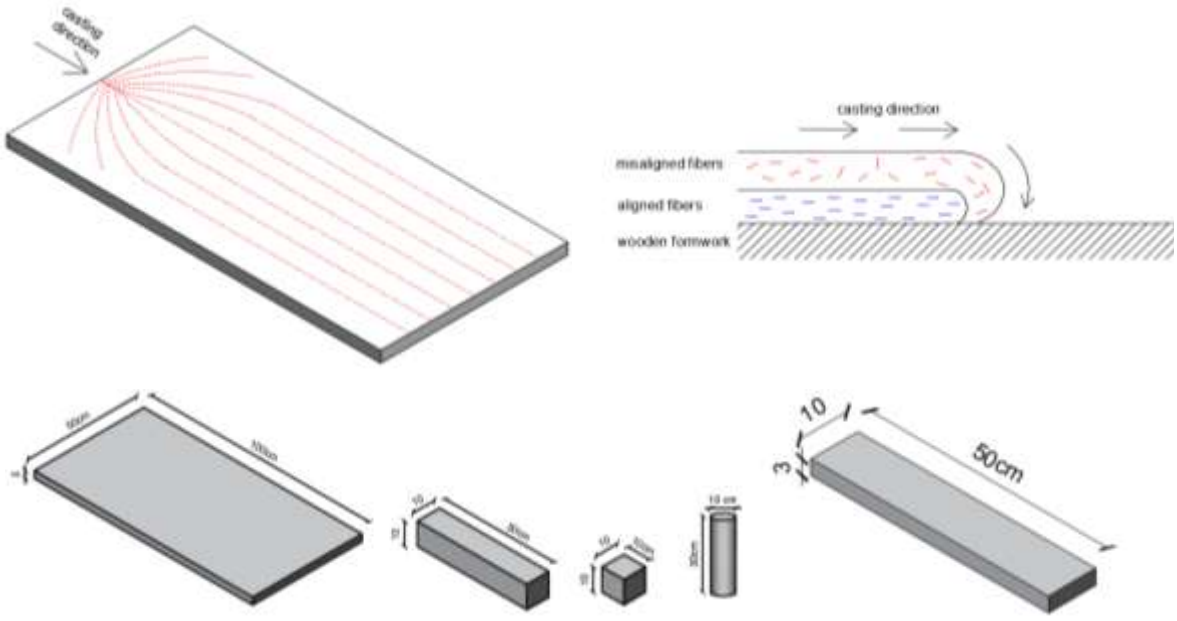

Figure 3. Specimen casting procedure and geometry of specimens casted (slab, prismatic specimens, cubes and cylinders). Thin beams (30x100x500mm^3) were obtained by saw-cutting from the casted slab.

As shown in Figure 4 the 20 thin beams were used for different tests. 8 thin beams were chosen for mechanical tests: 6 thin beams to be monotonically tested up to failure and 2 following a loading/unloading cyclic protocol at 0.5mm COD intervals (as shown in Figure 5) to calibrate

the evolution of the loading/unloading stiffness to be applied in the precracking tests on thin beams. Both tests were performed employing the 4-point bending test set-up shown in Figure 6. The remaining 12 thin beams were used to analyze self-healing behavior, to whose purpose the specimens were pre-cracked employing the same test setup shown in Figure 6.

Tests were carried out by means of a Instron 8562 machine under displacement control, at a speed equal to 3μm/s for prismatic specimens and 15μm/s for thin beams. Crack opening displacement (COD) was measured in the center of the specimen, intended as the cumulative measurement of all the microcracks generated in the central span of the thin beam, as expected for an Ultra High Performance Fiber Reinforced Concrete (UHPFRC).

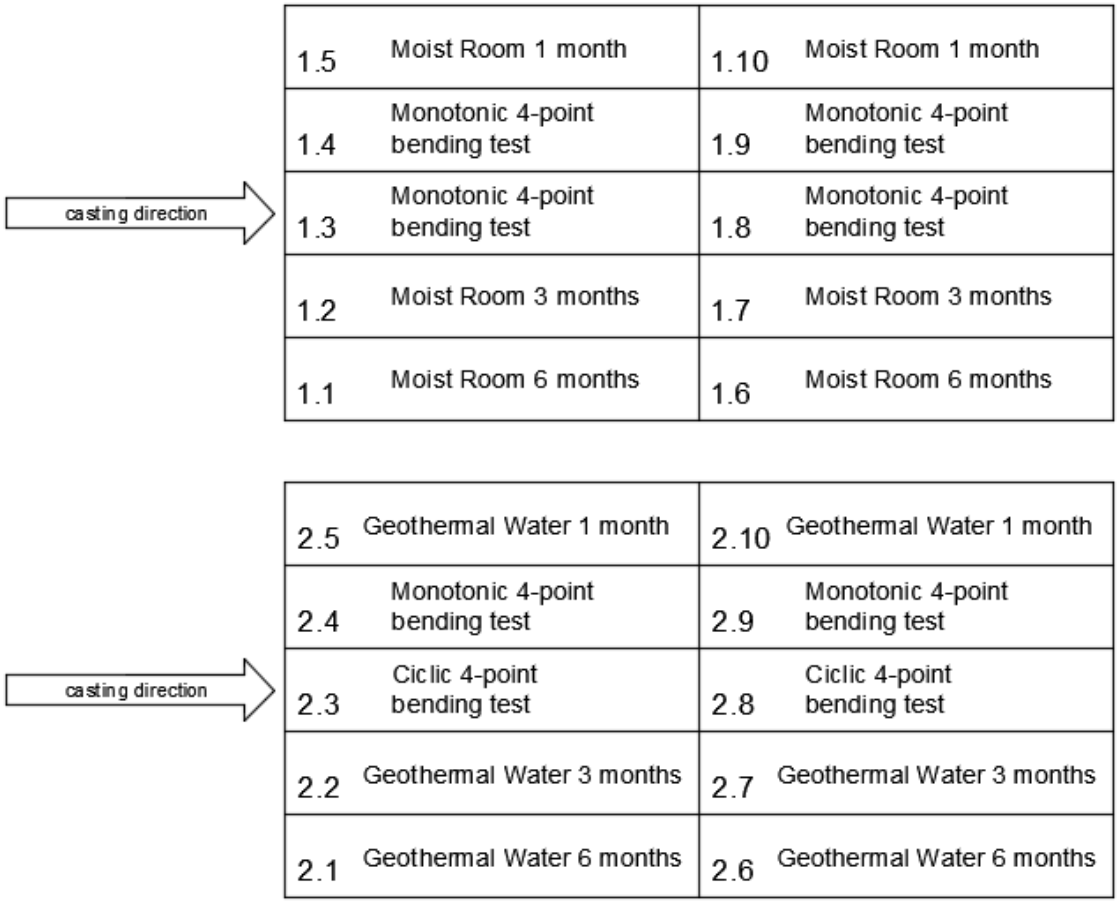

Figure 4. Thin beams: Identification inside the former slab

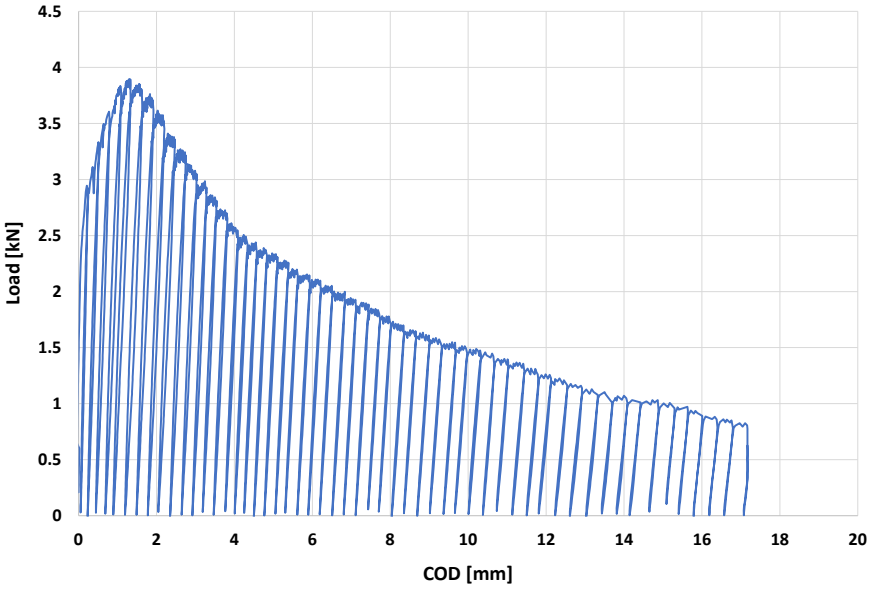

Figure 5. Loading/unloading cyclic protocol

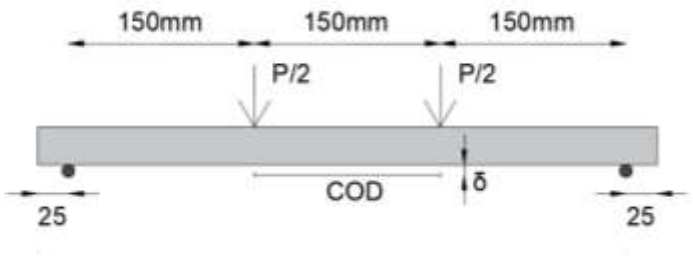

Figure 6. 4-point bending test setup.

As previously mentioned, self-healing was also characterized on specimens cured in moist room and immersed in geothermal water (rich in chlorides and sulfates) at laboratory temperature which composition is shown in Table 4. The identification of each thin beam and the corresponding test is shown in Figure 4. To analyze self-healing all thin beams were precracked up to a residual deformation equal to 1‰, equivalent to a cumulative residual crack opening value (COD) of 250µm. At the end, all precracking cracks were mapped with a digital microscope DinoLite® by means of its software DinoCapture®. For each specimen all cracks photographed with the microscope along all its length were analyzed. The crack width area was determined merging all the pictures using the software Photoshop Adobe Inc® (Figure 7).

Table 4. Composition of geothermal water.

Elements	**Al**	**Ca**	**Fe**	**K**	**Mg**	**Na**	**S**	**Si**	**SO_4**	**Cl**
ppm	0.2	4.0	0.1	19.8	0.3	1243.2	1523.4	0.3	2678.0	440.9

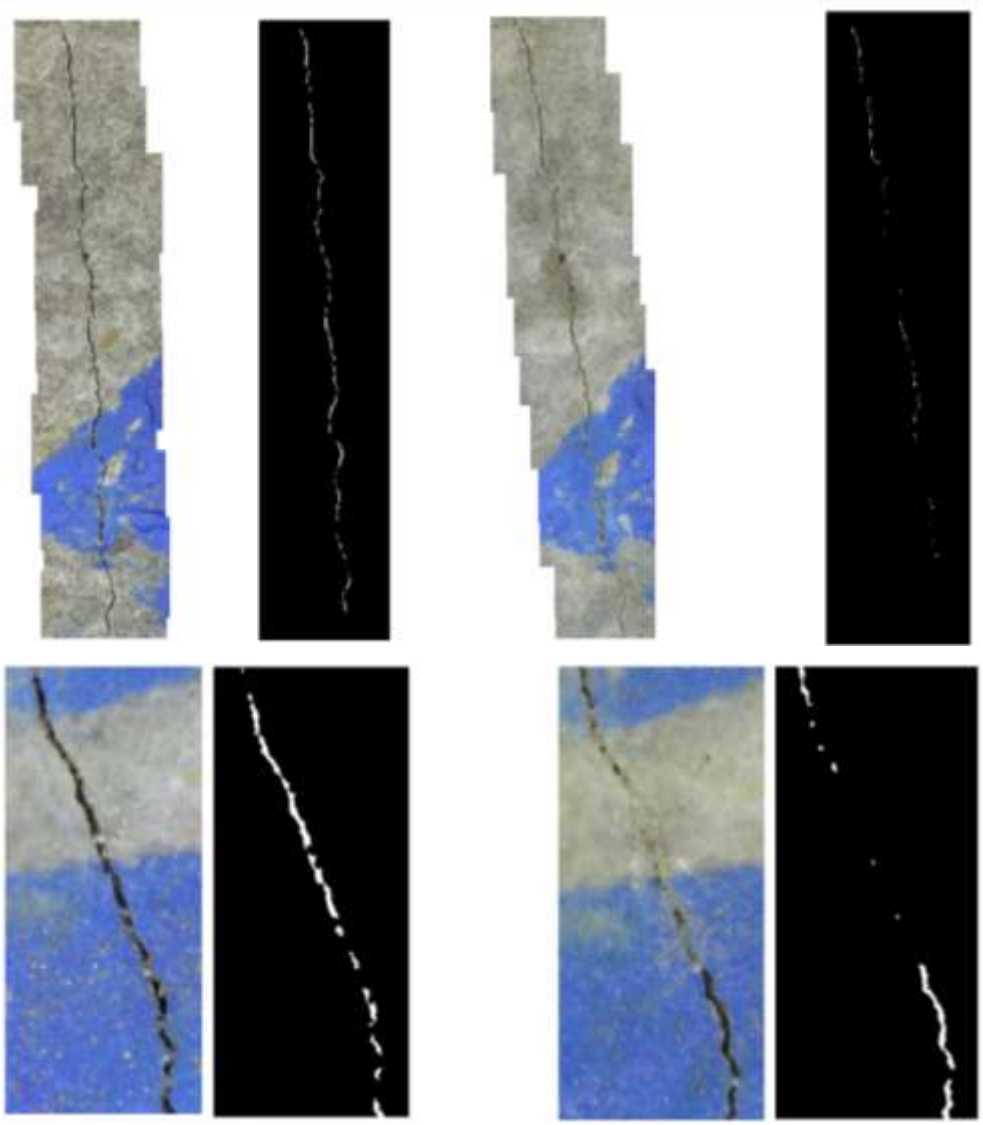

Figure 7. Example of crack monitoring and quantification of the crack area by means of black and white pixels

After microscope imaging, specimens were cured in moist room (thin beams: 1.1, 1.2, 1.5, 1.6, 1.7, 1.10) or immersed in geothermal water (thin beams: 2.1, 2.2, 2.5, 2.6, 2.7, 2.10) for 1, 3 and 6 months healing, as indicated in Figure 4. At the end of these periods, cracks were mapped again with the microscope to observe the crack sealing and were tested up to failure. Some of these thin beams were re-cracked as well after 1, 2 and 3 months and after re-cracking were cured again for 1, 2 and 3 months (see explanations in Table 5). Also for these specimens cracks were mapped at the end of each healing period (Figure 7).

Indirect tensile tests were also carried out. To this purpose Double Edge Wedge Splitting (DEWS) specimens were obtained from the following thin beams: 1.3, 1.4, 1.8, 1.9, 2.3, 2.4, 2.8 and 2.9 (Figure 4). As previously explained thin beams were tested up to failure. Then, the

extremes of the abovementioned thin beams were cut to obtain 10 DEWS specimens from the abovementioned thin beams. The extremes near to the casting point were discarded for DEWS since the alignment of fibers was clearly affected for the turbulence of that point. DEWS [46] tests allow to obtain tensile stress versus crack opening constitutive relationship of concrete without performing any inverse analysis. DEWS have a particular geometry with a notch and groove which determine the ligament cross section which can be parallel or orthogonal to the concrete flow direction (Figure 8). To further check the influence of fiber orientation on tensile behavior of concrete, DEWS with different fiber alignments were chosen resulting ligament cross sections either parallel (PL) or orthogonal (PD) to the mix flow direction (Figure 8). The DEWS geometry and test set-up is designed to subject the ligament to a pure mode I tensile stress state. It is expected to observe a hardening behavior for the DEWS whose ligament is orthogonal to the flow direction (fiber direction), these are PD DEWS. On the other hand, it is expected a softening behavior for PL DEWS (ligament parallel to the flow direction).

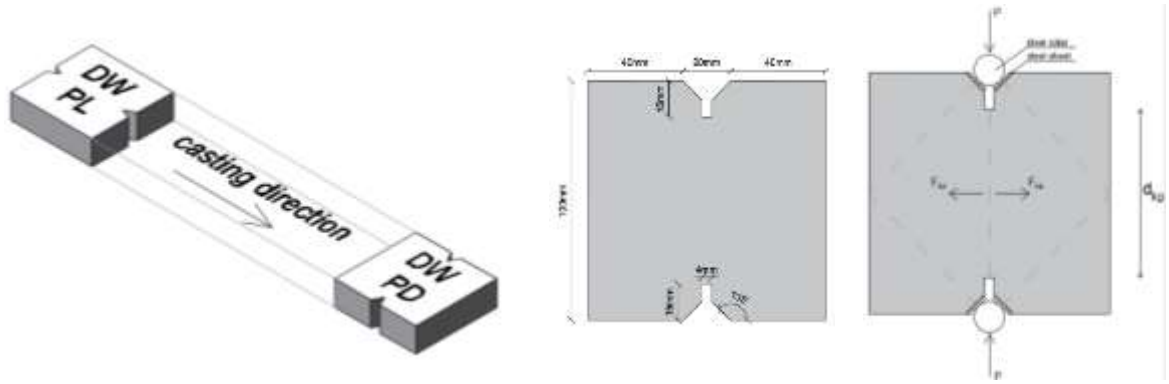

Figure 8. DEWS tests obtained from the thin beams

The cylinder specimens were cut into six disks 40mm thick for the permeability tests and nine disks 80mm thick for chloride diffusion tests.

For permeability tests disks were previously pre-cracked by means of splitting tension tests using the Instron 8562 machine in displacement control at a rate 0.5µm/s. Disks were pre-cracked up to a residual COD of 100-150µm on the surface. Each crack run through the entire disk from the loading point to the support. After pre-cracking and after healing periods, crack monitoring was carried out following the same methodology explained for the thin beams. Permeability tests were carried out following the test set-up shown in Figure 9 and analogous to [47], where a PVC pipe 500mm high was glued to one of the two surfaces of the disk with silicone. The silicone was also used to seal the lateral surface of the disk as well in other to

guarantee a unidirectional flow direction of water into the disk. The exact position of the PVC pipe was marked on the face of the disk for all disks, so that it could be repositioned exactly in the same place after each healing period. After each permeability measurement, both the PVC pipe and the silicone were removed from the specimen to be able to be immersed them in geothermal water. This methodology was repeated after 1, 3 and 6 months healing. The permeability test consists in measuring the quantity of water that passes through the cracked disk in different time intervals. To this purpose, the PVC pipe was filled up to have a 450mm high water column and the quantity of water which pass across the crack was collected and weighed after 5, 10, 20 and 30 minutes, for a total duration of 3 hours for each test (Figure 9).

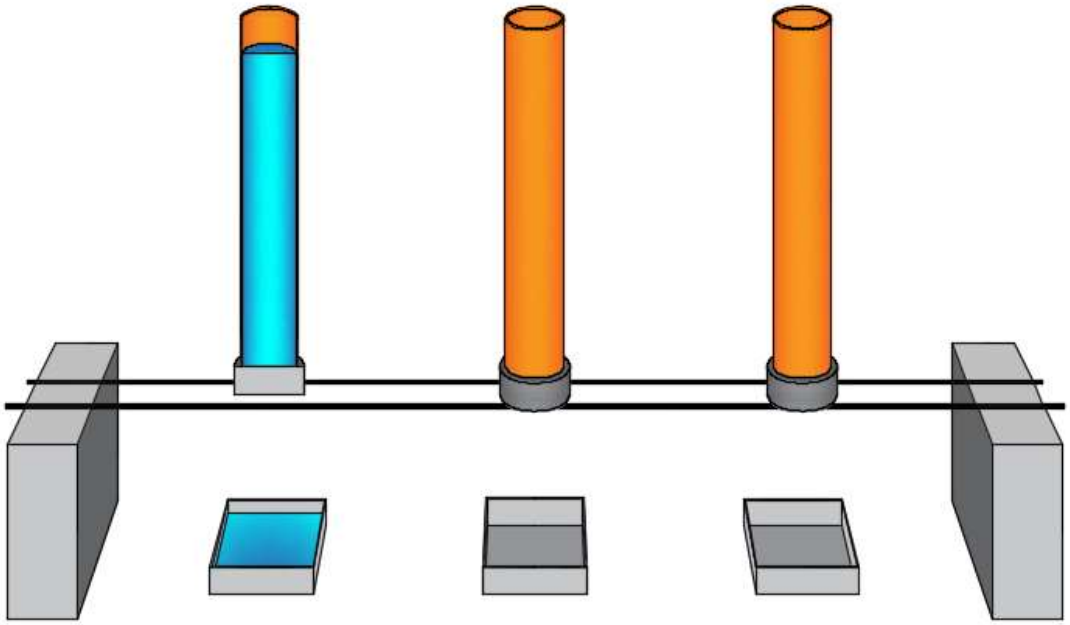

Figure 9. Test set-up for permeability tests

On the other hand, 80 mm thick disks were employed for chloride diffusion tests. To this purpose the surface of the cylinders were completely waterproofed except one of the circular faces to force a unidirectional flow direction of the salty water into the concrete cylinder. Subsequently, the cylinders were immersed in water with 33g/L of NaCl to simulate marine exposure for 1, 3 and 6 months. For each duration, 3 specimens were analyzed: one was kept un-cracked whereas the other two were cracked by means of splitting tests. The chloride content in concrete expressed in percentage of the concrete mass was determined by titration tests as per EN14629 (2007). To this purpose, concrete powder was obtained from the specimens drilling small 10 mm diameter cores at three different positions with respect to the crack as indicated in Figure 10. The whole experimental program is summarized in Table 5.

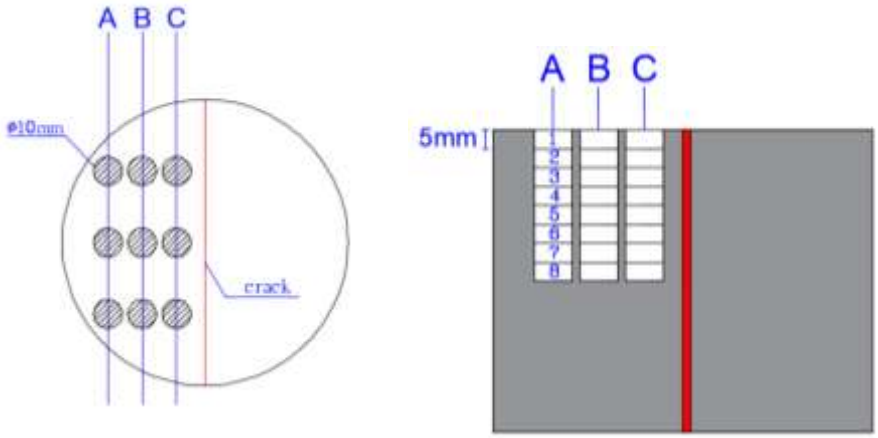

Figure 10. Position of the powder extraction points for the titration tests

Finally, the possible influence of cellulose nanofibers (CNFs) at a microstructural level was also analyzed by means of thermogravimetric analysis tests. Specifically, Thermogravimetry (TG), Derivative thermogravimetry (DTG) and Differential Thermal Analysis (DTA) were carried out on UHPFRC with CNFs and also on samples of the same UHPFRCs but without CNFs to better understand if there was any difference due to the presence of CNFs.

X-ray diffraction (XRD) tests were also carried out on the concrete under study (UHPFRC+CNF) and its corresponding reference concrete without nanoadditions (UHPFRC).

2.3. Definition of healing indices

Specific indexes were calculated using the results obtained from the experimental tests to quantify the mechanical and self-healing performance. The indices are described in Table 6. The Index of Crack Sealing (ICS) shows the crack sealing on the surface of the specimen. Three indices were defined and calculated to quantify the self-healing performance in both terms, impermeability (Index of Permeability Healing, IPH) and mechanical recovery by means of the Index of Stress Capacity Recovery (ISR) and the Index of Stiffness/Damage Recovery (IDaR) which were determined as graphically explained in Figure 11. A value equal to 1 for the different indices mean a total recovery of the related performance, this is, a specimen totally healed would reach the same properties than an uncracked one.

Table 5. Experimental program

Mechanical tests				
-8 cubes 100x100x100mm (compressive strength) -6 prismatic beams 100x100x500mm (4-point bending tests): 4 monotonic tests (up to failure) + 2 cyclic tests -8 thin beams 100x500x30mm (4-point bending tests): 6 monotonic tests (up to failure) + 2 cyclic tests -10 DEWS tests (indirect tensile tests).				
Self-healing and durability tests				
Test	**0 Months (T0)**	**1 Month (T1)**	**3 Months (T3)**	**6 Months (T6)**
4-point bending thin beams (12 specimens)	- 12 specimens pre-cracked [(1)]	- 4 specimens tested up to failure - 8 specimens re-cracked[(1)]	- 4 specimens tested up to failure - 4 specimens re-cracked[(1)]	- 4 specimens tested up to failure
Water permeability[(2)] (6 disks)	- 6 specimens pre-cracked	- 6 permeability tests performed	- 6 permeability tests performed	- 3 permeability tests performed
Chlorides diffusion[(3)] (9 cylinders)	- 6 specimens pre-cracked - 3 specimens immersed in salt water	- titration test of 2 pre-cracked and 1 uncracked specimens	- titration test of 2 pre-cracked and 1 uncracked specimens	- titration test of 2 pre-cracked and 1 uncracked specimens

[(1)] half of the specimens were immersed in geothermal water, the other half were stored in the moist room; [(2)] all specimens were immersed in geothermal water; [(3)] all specimens were immersed in salty water (33 g/L NaCl).

Table 6. Indices for quantification self-healing performance

Index	**Parameters**
Index of Crack Sealing (ICS): $ICS = 1 - \frac{A_{crack,t}}{A_{crack,0}}$	$\boldsymbol{A_{crack,t}}$: area of the crack at a certain time "t" $\boldsymbol{A_{crack,0}}$: initial crack area (just after precracking and before healing curing).
Index of Permeability Healing (IPH): $IPH = 1 - \frac{K_t}{K_0}$	$\boldsymbol{K_t}$: permeability coefficient at a certain time "t" $\boldsymbol{K_0}$: initial permeability coefficient where $\boldsymbol{K}$ is the slope of the volume of water which has passed across the crack vs. time curve
Index of Stress Capacity Recovery (ISR): $ISR = \frac{\sigma_{peak,recracked} - \sigma_{virgin}^{scale}}{\sigma_{virgin}^{scale}}$	*(the determination of the different parameters is graphically explained in Figure 11)*
Index of stiffness/Damage Recovery (IDaR): $IDaR = \frac{K_{loading,recracking} - K_{unloading,precracking}}{K_{loading,precracking} - K_{unloading,precracking}}$	*(the determination of the different parameters is graphically explained in Figure 11)*

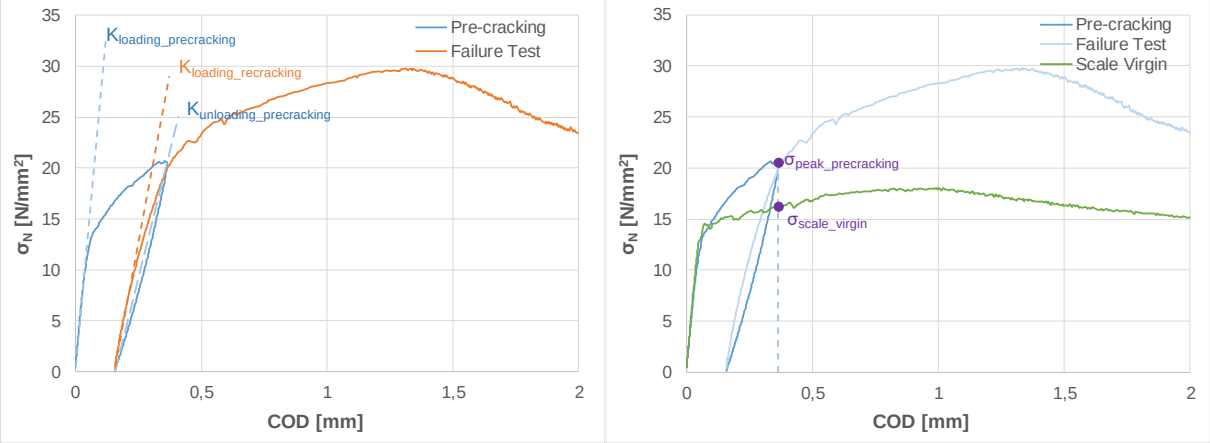

(a) (b)

Figure 11. Scheme to determine the parameters involved in the calculation of ISR and IDaR

3. ANALYSIS OF RESULTS

The mechanical and self-healing behavior of UHPC with CNFs have been studied in this research. In the present section, the results are shown and analyzed. The reference UHPC (same mix without CNFs) has been already studied in depth by the same research group [17].

3.1. Mechanical behavior

The mechanical behavior of the investigated UHPFCRs with CNFs was characterized by means of compressive strength tests, indirect tensile tests via DEWS methodology and flexural strength tests via 4-point bending tests.

Compressive strength was tested on 100x100x100mm cubic specimens and the average value at 293 days was 127.21 MPa with a coefficient of variation (CoV) of 8%. The prolonged curing time was due to COVID-19 pandemic. The same mix with alumina nanofibers instead of CNFs had a similar average value of compressive strength being 131 MPa [10].

4-point bending tests were performed on 500x100x30mm thin beams and on 100x100x500mm prismatic beams (Figure 12). Indirect tensile tests were carried out on DEWS tests (Figure 13). As shown in Figure 12 flexural tests on both thin and deep beams (100x100x500mm) featured a good repeatability with an admissible scattering for flexure tests. The scattering was quantified by means of the coefficient of variation (%) shown in Table 7. For both types of beams (thin and deep) the average maximum stress values were very similar (around 19 MPa) and the coefficient of variation, CoV was around 13% in both cases, as indicated in Table 7.

The results of DEWS tests confirmed on the one hand the role of fiber alignment in guaranteeing, when favorable (i.e. orthogonal to the fracture plane/parallel to the tensile stress),

a strain hardening behavior (Figure 13a) whereas when fibers were oriented parallel to the ligament a softening behavior (Figure 13b) was obtained. Table 8 contains the maximum stress values reached by each DEWS specimen indicating their behavior, softening or hardening, as well as the average stress value and the coefficient of variation for each kind of behavior. As a matter of fact, DEWS specimens characterized by a hardening behavior reached higher stress values (average=10.77 MPa) compared with the softening ones (6.17 MPa). As expected, a favorable fiber alignment also resulted into a reduced scattering, CoV equal to 11.01% for hardening specimens versus 16.08% for softening specimens (Figure 13).

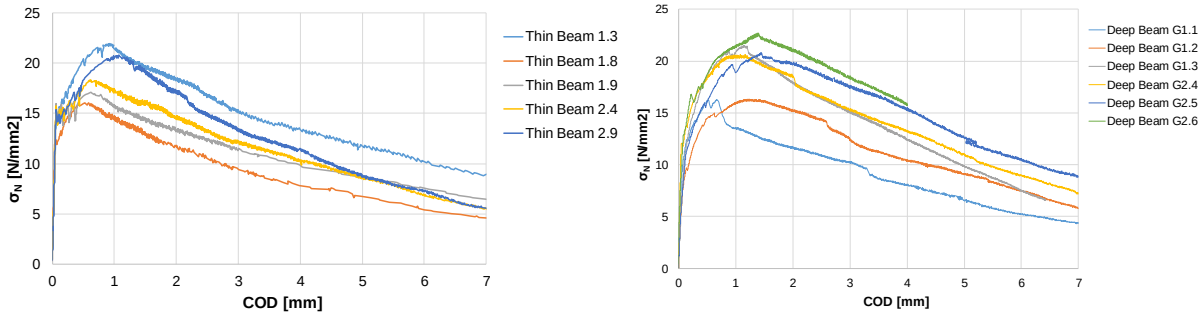

(a) (b)

Figure 12. Nominal flexural stress vs. COD curves from thin beams (a) and deep prismatic beams (b) subject to four-point bending tests.

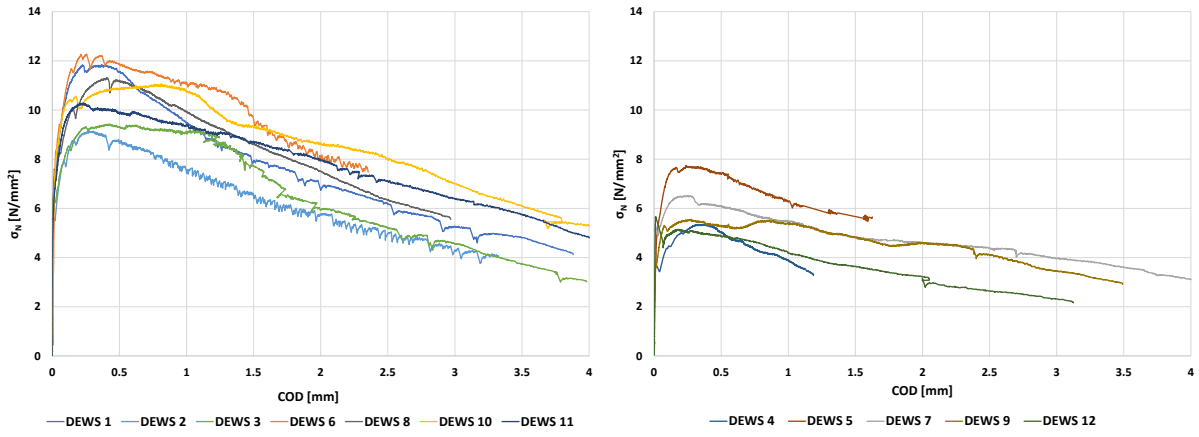

(a) (b)

Figure 13. Tensile strain-hardening (a) vs. softening (b) response of DEWS specimens

From the results of DEWS tests a multilinear tensile stress versus strain constitutive law was determined assuming a quadrilinear relationship in tension following a normal stress distribution in five stages as explained in [13]. Using that as an input and using force and

moment equilibrium equations the flexure behavior of prismatic (deep) beams was simulated as showed in Figure 14. The analytical curve simulated very well the behavior of the experimental curves. As a matter of fact, the analytical curve was very close to the average experimental curve, specially before the peak. It proves the reliability of DEWS tests to provide the constitutive law of the material without performing any kind of inverse analysis. Moreover, the abovementioned constitutive law provided a reliable input to obtain a good simulation of the flexure response of the prismatic beams.

Table 7. Maximum stress values obtained from flexural tests on thin and deep beams

Type of specimen	**Specimen ID**	**$\sigma_{N,MAX}$ [MPa]**	**Average $\sigma_{N,MAX}$ [MPa] (Coefficient of variation, CoV in %)**
Thin beam	1.3	21.98	18.68 (13.53%)
	1.8	15.81	
	1.9	17.03	
	2.4	18.09	
	2.9	20.51	
Deep beam	G1.1	16.28	19.72 (13.94%)
	G1.2	16.31	
	G1.3	21.51	
	G2.4	20.67	
	G2.5	20.82	
	G2.6	22.72	

Table 8. Maximum stress values obtained from DEWS tests

Behavior regarding fiber orientation	**Specimen ID**	**$\sigma_{N,MAX}$ [MPa]**	**Average $\sigma_{N,MAX}$ [MPa] (Coefficient of variation, CoV in %)**
Hardening DW PD	DEWS 1	11.84	10.77 (11.01%)
	DEWS 2	9.16	
	DEWS 3	9.42	
	DEWS 6	12.27	
	DEWS 8	11.32	
	DEWS 10	11.07	
	DEWS 11	10.29	
Softening DW PL	DEWS 4	5.35	6.17 (16.08%)
	DEWS 5	7.75	
	DEWS 7	6.52	
	DEWS 9	5.56	
	DEWS 12	5.65	

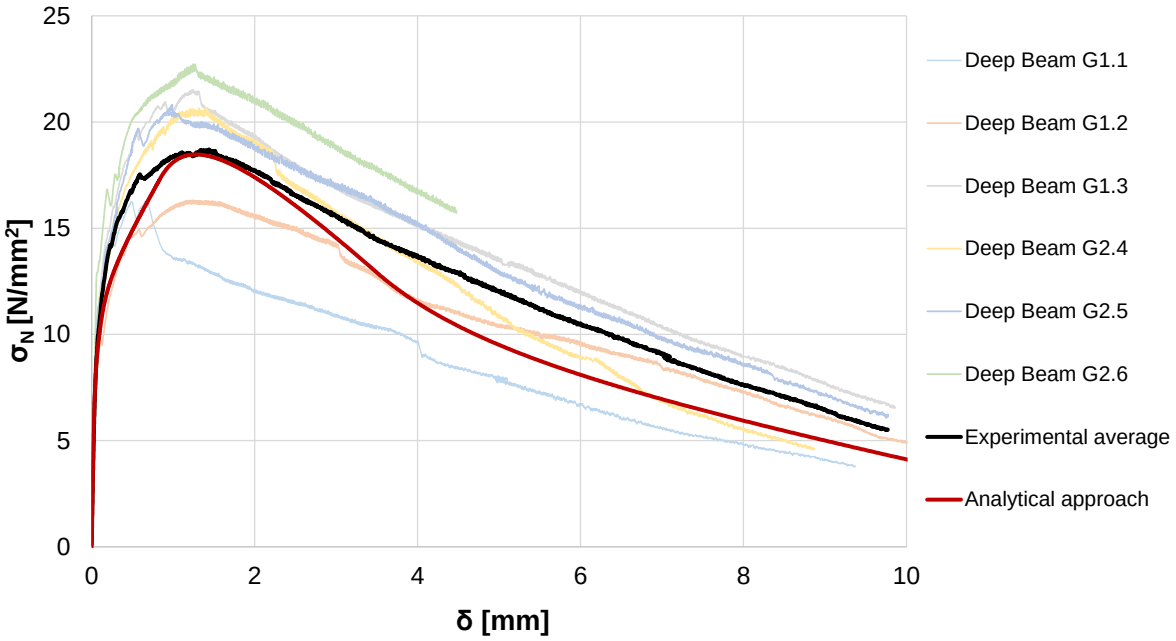

Figure 14. Nominal flexural stress vs. deflection. Comparison between experimental curves and analytical curve obtained from 5-point inverse analysis method [13]

3.2. Precracking of thin beams

As explained, twelve thin beams were pre-cracked to be subsequently subjected to curing either in moist room or immersed in geothermal water to further analyze self-healing behavior and the related mechanical performance recovery. Pre-cracking flexural nominal stress vs COD curves are shown in Figure 15. The average residual COD was 0.17mm. Considering that the average number of cracks in the central span (between supports) is 8 it can be hypothesized an average crack width equal to about 20µm. Table 9 summarizes the residual COD, the number of cracks and the average distance between cracks for each thin beam.

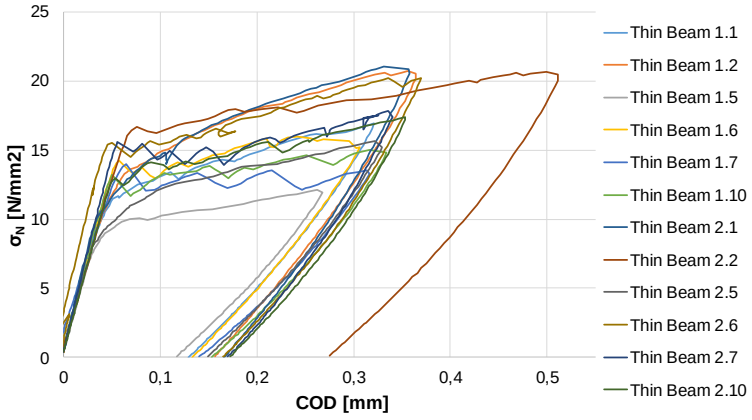

Figure 15. Pre-cracking tests on thin beams. Flexural nominal stress vs. COD curves

Table 9. Residual COD, number of cracks, average distance between cracks on thin beams

Specimen ID	Residual COD [mm]	Number of cracks	Average distance between cracks [mm]
Thin beam 1.1	0.1311	8	19
Thin beam 1.2	0.1567	8	19
Thin beam 1.5	0.1169	7	21
Thin beam 1.6	0.1324	7	21
Thin beam 1.7	0.1401	7	21
Thin beam 1.10	0.1531	6	25
Thin beam 2.1	0.1659	9	17
Thin beam 2.2	0.2751	7	21
Thin beam 2.5	0.1489	7	21
Thin beam 2.6	0.1650	6	25
Thin beam 2.7	0.1695	7	21
Thin beam 2.10	0.1721	6	25
Average (COV%)	0.1606 (24.89%)	7 (12.71%)	21 (11.88%)

3.3. Self-sealing (crack-closure) capacity

As previously explained the crack sealing capacity of the material was quantified through an Index of Crack Sealing, ICS (%), which was determined on two different types of specimens. In disks, ICS was determined after 1, 3 and 6 months healing immersion in geothermal water, whereas on thin beams ICS was determined in two different exposures, moist room and immersion in geothermal water. The main difference between disks and thin beams is that the first were pre-cracked and then remained for 1, 3 and 6 months immersed in water whereas thin beams were exposed to the abovementioned conditions for 1 months and then were re-cracked again to be healed two months more (1+2 month), after 2 months of exposure were re-cracked again and then were subjected to the exposure conditions for 3 months more (1+2+3 months). The ICS (%) with respect to the initial crack width (μm) in thin beams cured in moist room and geothermal water are shown in Figure 16a and Figure 16b, respectively. It can be observed that ICS is higher when specimens were immersed in geothermal water compared to moist room condition. For specimens immersed in geothermal water ICS values ranged from 30 to 93% whereas for moist room ranged from 14 to 80% for the same range of initial crack width (4-40μm). After 1 month, the average value of ICS for moist room was 30% whereas the average value reached 60% for immersion in geothermal water. This confirmed that the complete immersion in water was highly positive in terms of self-sealing. Moreover, the highest ICS values were obtained after 1+2 months. However, after 1+2+3 months the re-cracking effect affected the crack sealing since the crack had been reopened for three times and the remaining unhydrated cement particles were lower than in previous stages, which affected directly to the

sealing capacity. This decreasing of sealing efficiency can be also clearly observed in Figure 17 for all the studied ranges of crack width and for both investigated exposure conditions. Still, also after three (p)re-cracking/healing cycles the material keeps a crack sealing capacity generally higher than after the first pre-cracking and healing treatment, likely because of a combined synergy among its peculiar composition (large availability of unhydrated binder), the long-term effects of the crystalline admixture [44] and the internal curing role played by the nano-cellulose.

When specimens were pre-cracked and then continuously immersed in geothermal water for 1, 3 and 6 months, without intermediate re-cracking (this is the case of disks used for permeability tests), ICS value increased with the duration of the healing exposure. Moreover, the wider the crack width, the lower the sealing, as expected and shown in Figure 18.

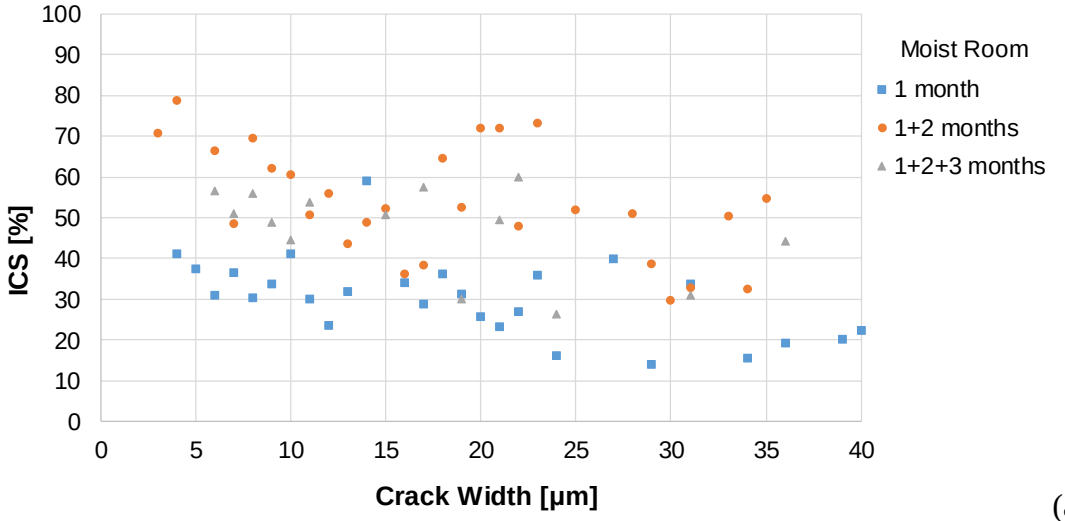

(a)

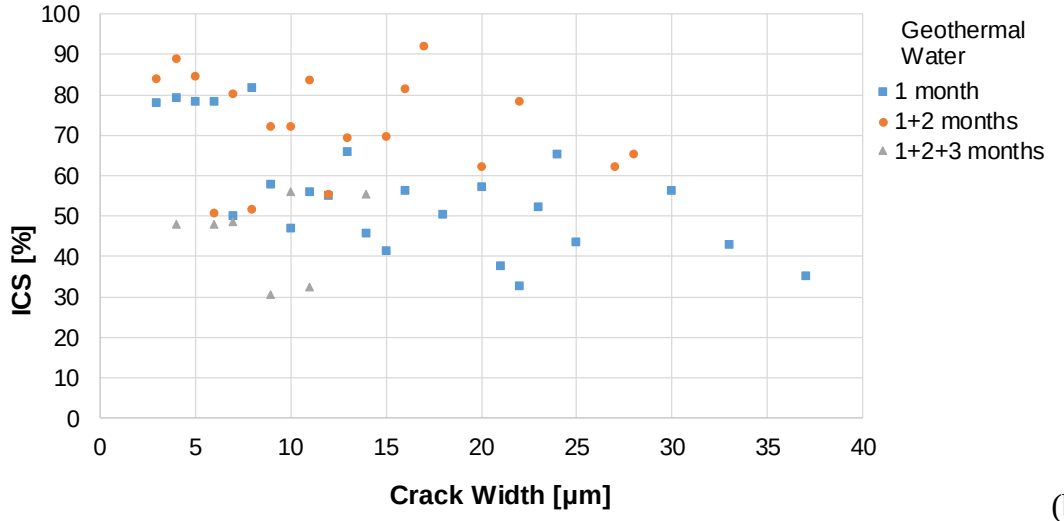

(b)

Figure 16. Index of Crack Sealing vs. initial crack width for different curing times of thin beams cured: in moist room (a) and immersion in geothermal water (b)

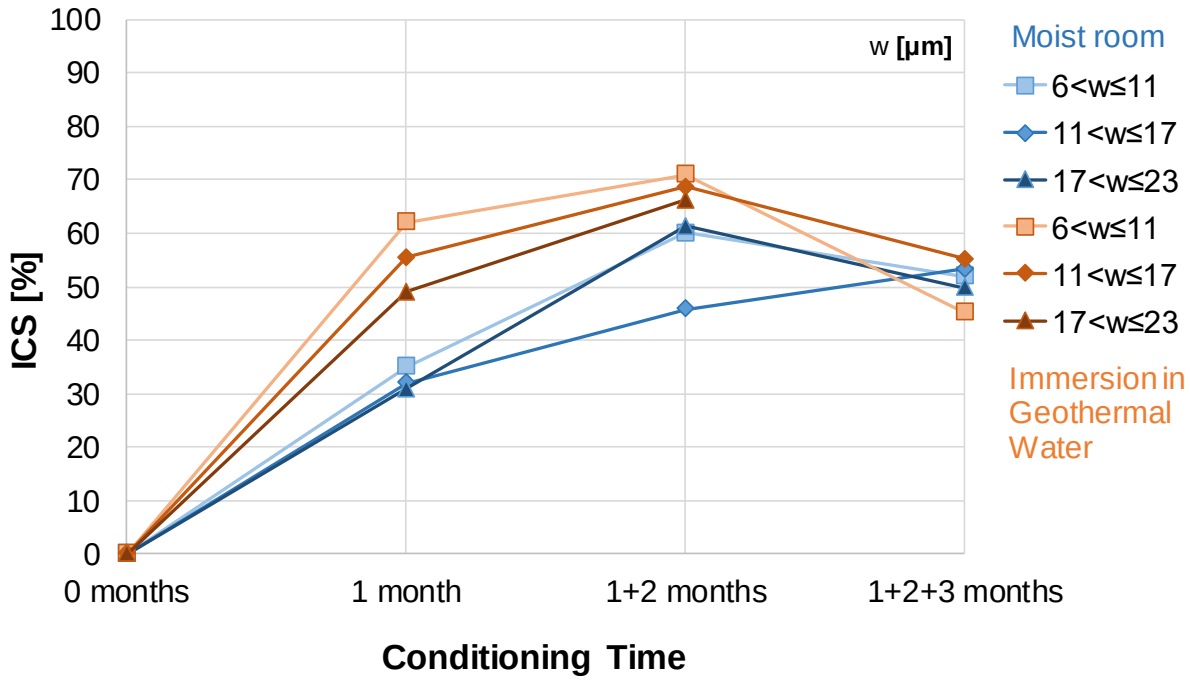

Figure 17. Index of Crack Sealing vs. time and crack width on thin beams

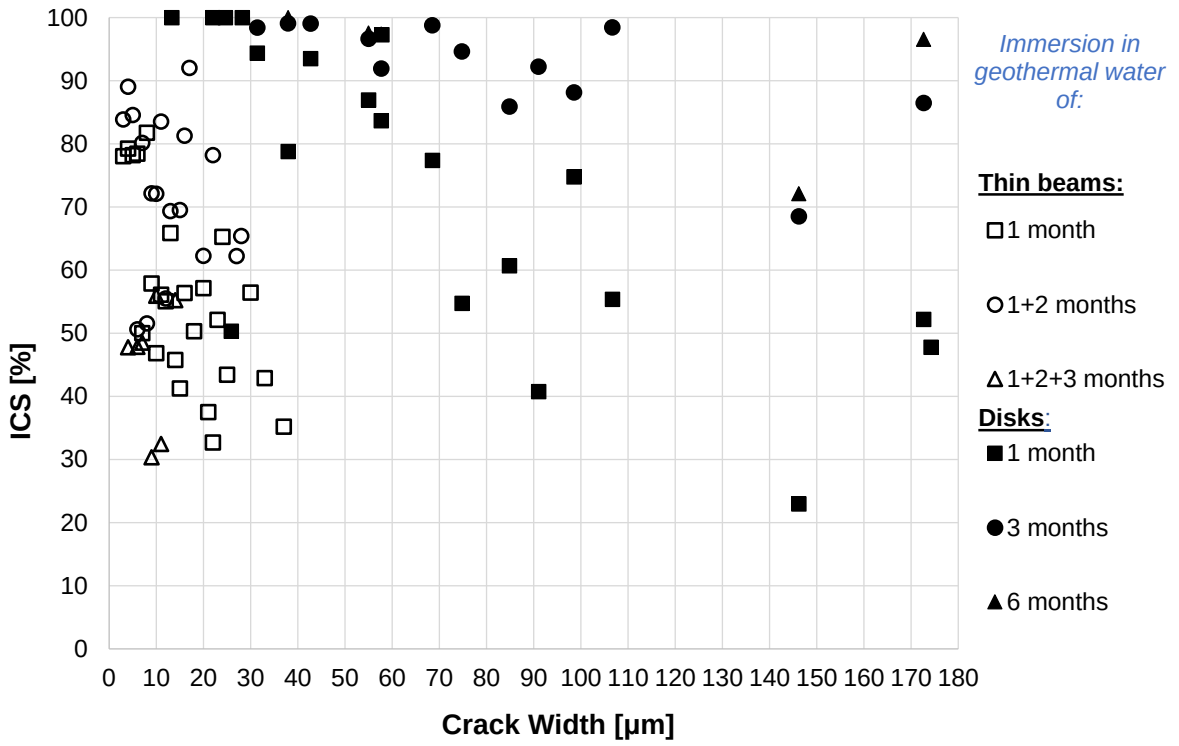

Figure 18. ICS [%] vs Crack Width [µm] tested on thin beams and disks immersed in geothermal water

Figure 18 shows ICS values vs. crack width for all the specimens immersed in geothermal water, these were disks and thin beams. For a same value of crack width and after 1-month

healing, disks reached higher ICS values than thin beams. This is reasonably since, disks were precracked by splitting and the crack was opened at both sides of the disk allowing the entrance of geothermal water for healing from both sides of the specimens. As a matter of fact, this accelerates the hydration of unhydrated cement particles in the inner part of the specimen. On the other hand, the cracks on thin beams were only open on one side being the entrance of water slower than for disks (with a double entrance of water).

Moreover, it is well known that the crack width created by splitting tests is more difficult to control than a crack obtained from flexure tests. Consequently, the crack widths obtained by splitting were wider than those obtained with flexure tests, this is the case of disks and thin beams respectively. The crack width on thin beams ranged from 5 to 40 μm whereas for disks ranged from 12 to 175 μm. All these effects can be clearly observed in Figure 18.

In order to analyze the effect of CNFs on self-healing, the values obtained in the present experimental campaign were compared with a parallel experimental campaign where specimens made with the same concrete mix but without nanoadditions [17] and same concrete mix with alumina nanofibers (ANFs) [10]. All these mixes were investigated, in the framework of the H2020 Reshealience project [17], [10], [16], [5]. The comparison is shown in Figure 19. The presence of nanocellulose (CNFs) has resulted very positive in terms of self-sealing since for a same crack width value and same healing period (1, 3 or 6 months) the specimens with CNFs reached higher ICS values compared to those without nanoadditions and to those with ANFs. Moreover, an ICS value of 100 % was only reached for specimens with CNFs and quite irrespectively of the initial crack width. This is likely to confirm the role of CNFs as promoters of internal curing and conveyors, throughout the UHPC volume, of the water (which is the main healing agent) thus promoting a more spread and effective activation of the delayed hydration and of the crystalline admixture reactions at the basis of the self-healing process. Interestingly, a further comparison can be made with the results obtained by Cuenca et al. [10] where the same UHPC mix but containing alumina nanofibers (ANF) was tested according to the same herein described and employed rationale. It can be argued, from the results, also shown in Figure 19, that the main benefit obtained from the addition of ANF stands in an enhanced toughening of the material response, which leads in any case to thinner cracks, which are, as a matter of fact, easier and faster to be healed.

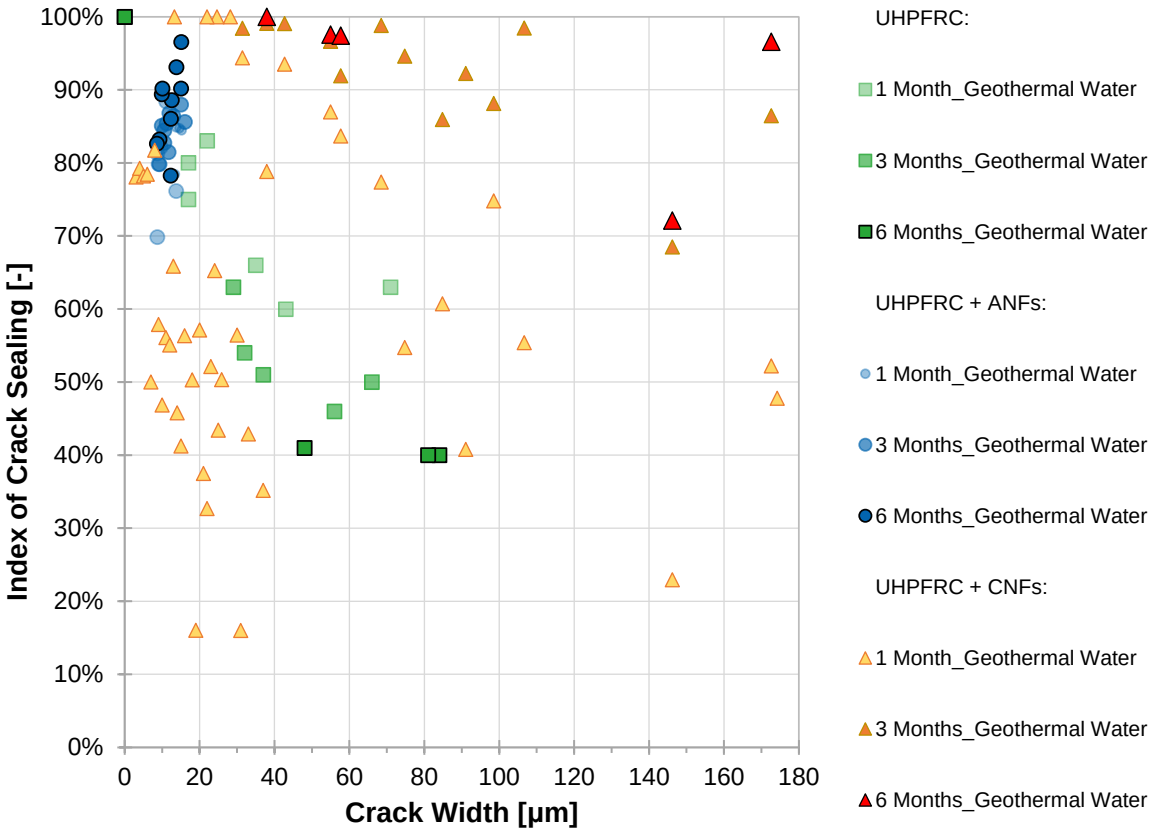

Figure 19. Index of Crack Sealing (ICS) vs. crack width. Comparison with the same mix without nanoadditions, with alumina nanofibers (ANF) and cellulose nanofibrils (CNFs)

3.4. Self-healing (performance recovery) capacity

3.4.1. Recovery of mechanical properties

As previously explained the recovery of mechanical properties was also evaluated, as an effect of self-healing. The values of the healing indices ISR an IDaR versus initial crack width are represented in Figure 20 and Figure 21 respectively. Focusing on cracks with openings ranging from 8 to 16µm, the highest values of ISR were reached when specimens were immersed in geothermal water for both, precracked (1 month) and recracked (1+2 months) specimens. Moreover, the ISR value decreased with the crack width (Figure 20), as expected, as well as IDaR (Figure 21). IDaR values after 1-month healing were very similar for both exposures (moist room and immersion in geothermal water). After recracking, no significant differences were observed for both types of exposure.

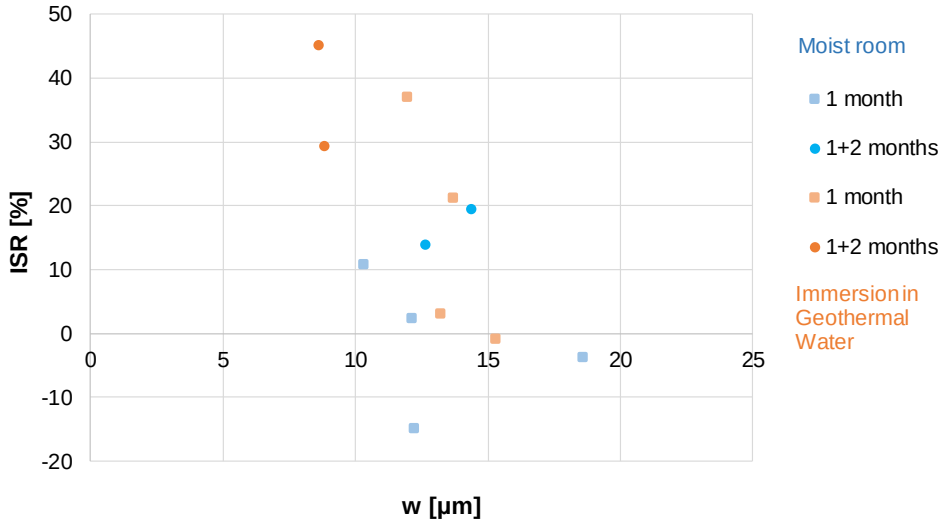

Figure 20. Index of Strength Recovery for different initial crack widths along healing time

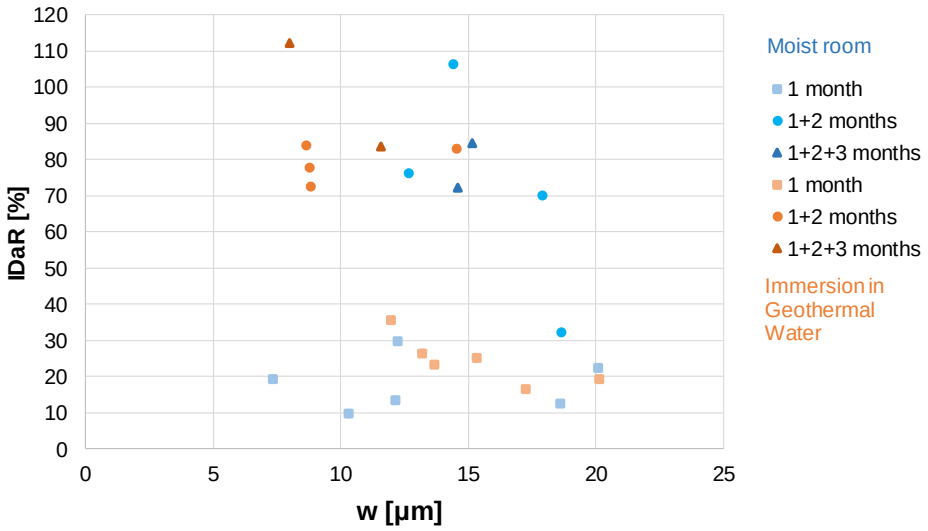

Figure 21. Index of Stiffness Recovery for different initial crack widths along healing time

Moreover, the indices of Strength Recovery and Damage Recovery obtained from the experimental tests from UHPC with CNFs were compared with other experimental values obtained from previous own studies [10], [17] made with the same concrete without nanoadditions and the same concrete with a different type of nanoadditions, alumina nanofibers (ANFs). Those comparisons are plotted in Figure 22 and Figure 23 respectively.

Although the healing periods were not exactly the same, from Figure 22 it seems that for a same range of crack width the UHPC with ANFs reached higher Indexes Strength Recovery values compared to those with CNFs. Moreover, an increase of the Index Strength Recovery due to the presence of CNFs was not observed compared to UHPC without nanoadditions. As a matter of fact, alumina nanofibers (ANFs) increase concrete toughness whereas cellulose

nanofibers (CNFs) merely accelerate the crack closure mechanism without increasing the mechanical recovery.

On the other hand, regarding the Index of Damage Recovery, the values were very similar for both types of nanoadditions, ANFs and CNFs.

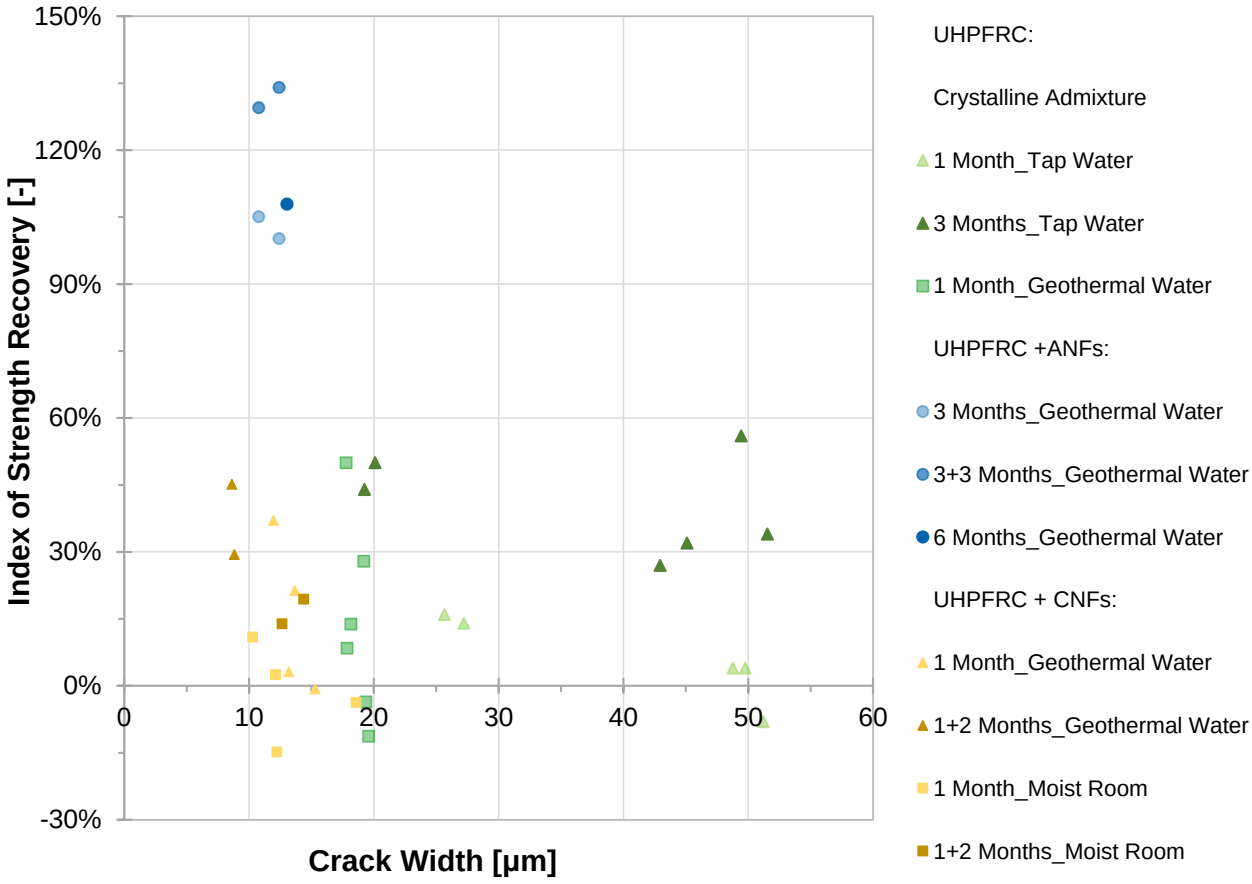

Figure 22. Index of Strength Recovery vs crack width. Comparison with UHPC with and without nanoadditions (ANFs and CNFs)

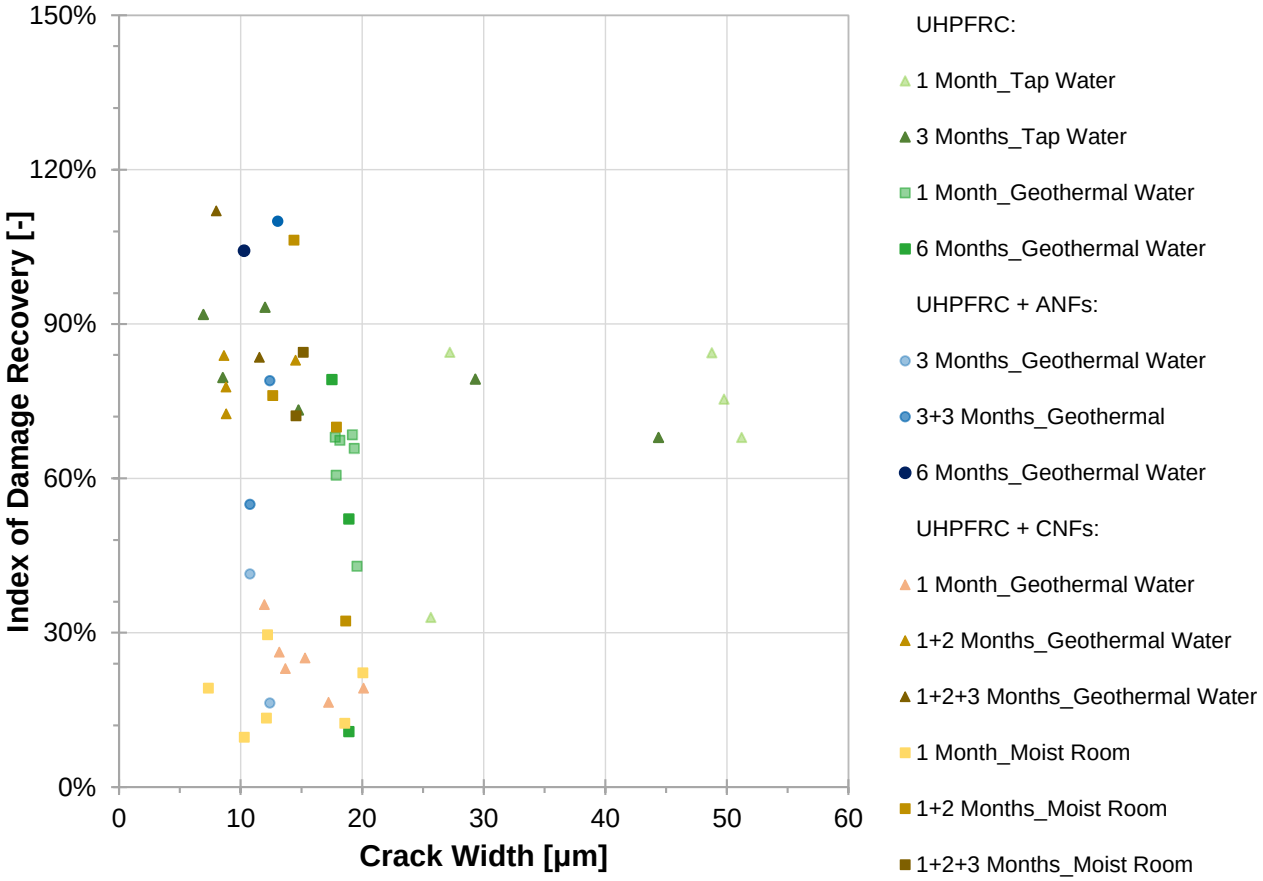

Figure 23. Index of Damage Recovery vs crack width. Comparison with UHPFRC with and without nanoadditions (ANFs and CNFs)

3.4.2. Recovery of impermeability via water permeability tests

The water flow (ml/min) versus crack width is shown in Figure 24. As expected, the water flow in healed specimens was lower than precracked ones (preconditioning) since the cracks became narrower the longer the healing time was. However, three specimens were completely sealed after 3 months. Therefore, after 6 months, only 3 specimens remained for analyzing permeability. The Index of Permeability Healing (IPH) reached a 100% when a crack was completely healed (Figure 25a). In Figure 25b the IPH was plotted vs. crack width. The IPH was inversely proportional to crack width as expected, since when the crack width increased, the IPH decreased. Moreover, for the same value of crack width the water flow after 6 months healing was zero since the cracks were completely healed. This effect was also clearly observed in Figure 25b.

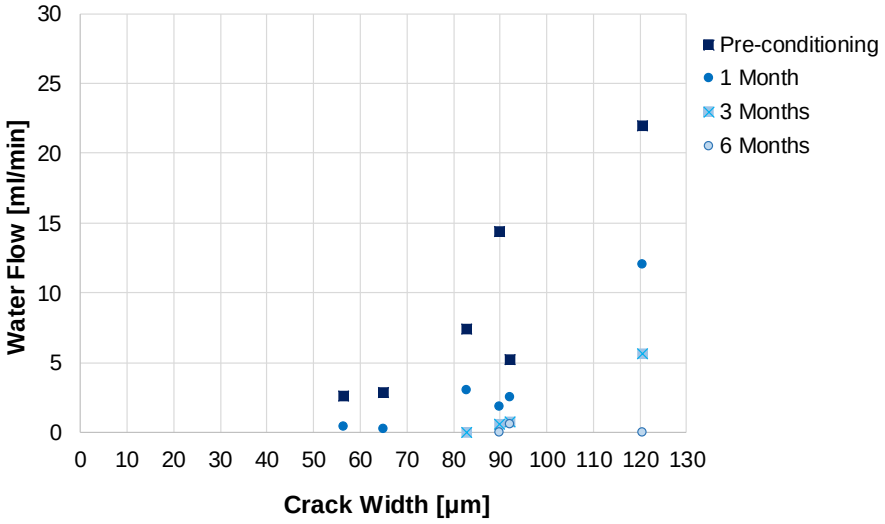

Figure 24. Water flow rate vs. initial crack opening in permeability tests

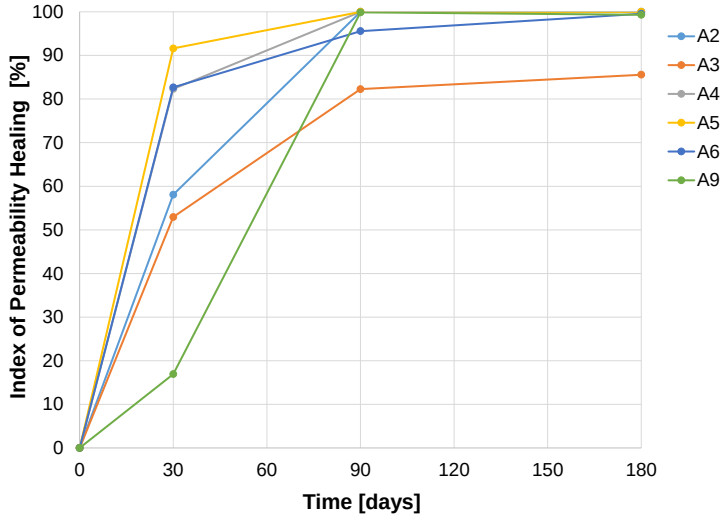

(a)

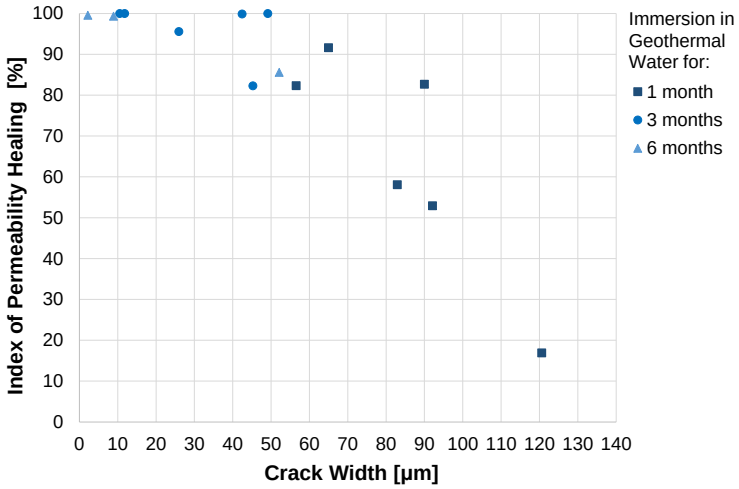

(b)

Figure 25. Index of Permeability Healing vs. healing time (a) and vs. crack width (b)

The Index of Permeability Healing (IPH) was also correlated with the Index of Crack Sealing (ICS) for specimens immersed in geothermal water for 1, 3 and 6 months (Figure 26). As expected, both indexes were directly proportional since when Index of Crack Sealing increased, the Index of Permeability Healing also increased. The longer the healing time, the higher the value of both indices. Moreover, this relationship between indexes was also compared with UHPC without nanoadditions, in order to evaluate the effect of the CNFs. This comparison can be observed in Figure 26 in which the average values for each concrete type and each curing period have been represented. The presence of CNFs improved the Index of Permeability which means better sealing of healing of cracks when CNFs were present. The positive contribution of CNFs could be observed after 30 days of immersion in geothermal water as showed in Figure 27. After 90 and 180 days, 3 and 6 months respectively, the positive effect of CNFs in terms of crack healing was clearly observed compared to the mix without nanoadditions. This substantially confirms the fact that the best self-healing performance found when CNFs were present depended precisely on the fact that the nanocellulose carries water and stimulates reactions, especially thanks to its specific surface. For instance, the amount of CNFs by m^3 of concrete was 0.9 kg (Table 1). Considering that CNFs have a specific surface of 31-33 m^2/g mean that the specific surface reaches 30000 m^2 dealing a higher specific surface compared to the mix without nanoadditions. Moreover, cement and slag have a specific surface of 0.35 m^2/g which is almost 100 times lower than the one of CNFs.

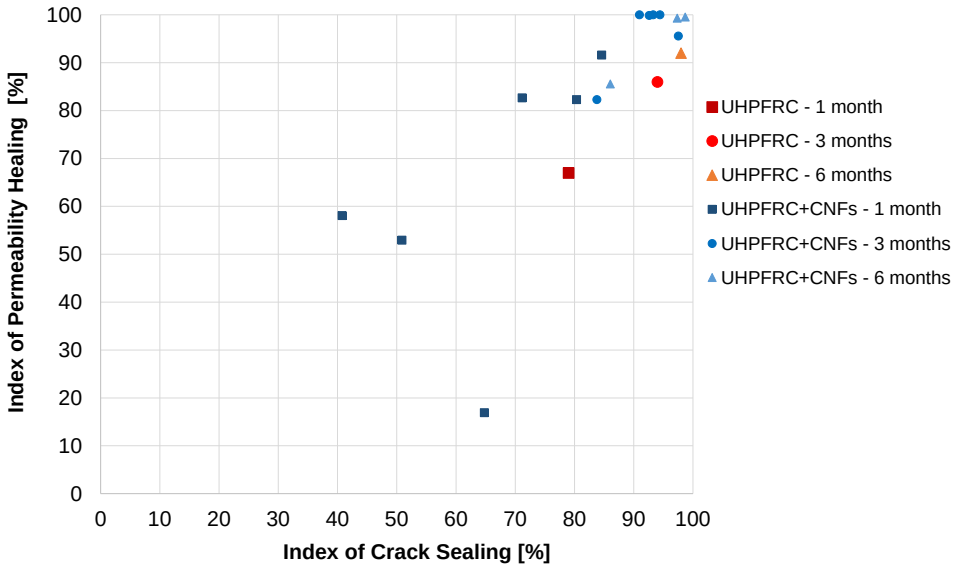

Figure 26. Index of Permeability Healing vs. Index of Crack Sealing: Comparison between UHPFRC with and without CNFs both immersed in geothermal water

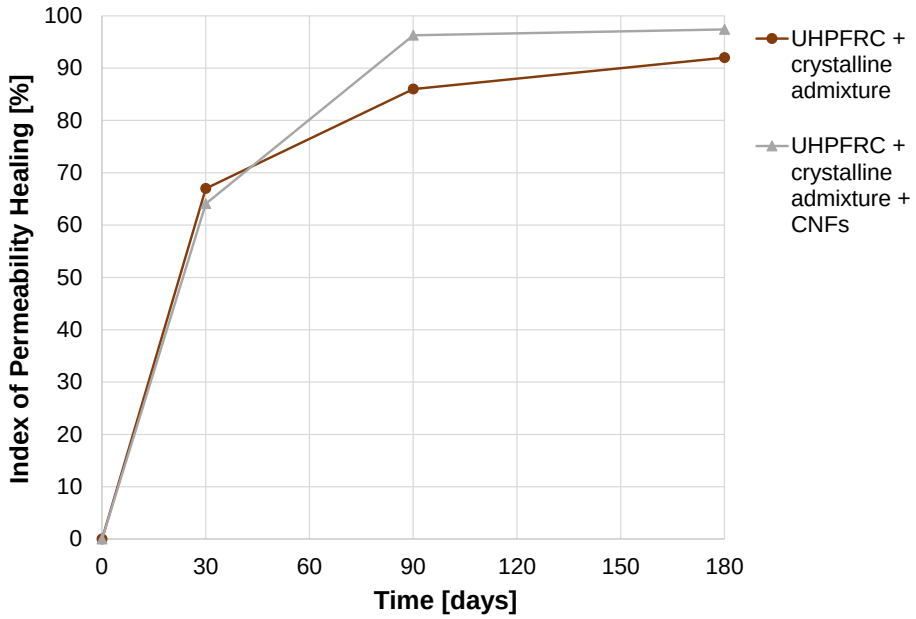

Figure 27. Index of Permeability Healing [%] vs. time [days]. Comparison with and without cellulose nanofibers (CNFs)

3.4.3. Chloride diffusion tests

As explained, chloride diffusion tests were carried out on 80mm thick cylinders immersed in salty water (33g/L of NaCl) for healing along 1, 3 and 6 months. Two cylinders were cracked by means of splitting tests and one specimen remained uncracked. The amount of chlorides was determined by titration tests according to the Standard EN 14629 (2007) and the results are showed in Figure 28.

No significant differences on chloride content between the position of the sample with respect to the crack (positions A, B, C) were observed. The chloride content in the first slice obtained at a depth equal to 0-5 mm was always the highest and its value increased with exposure time, as expected. In the inner layers, the chloride content remained constant after 3 and 6 months and at values comparable to those of uncracked specimens, since the crack was sealed on the surface for cracks, as from the values reported in the graphs in Figure 28.

1 month

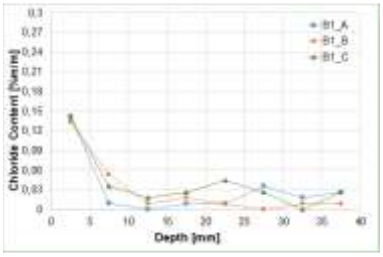

Initial crack width=86.9µm

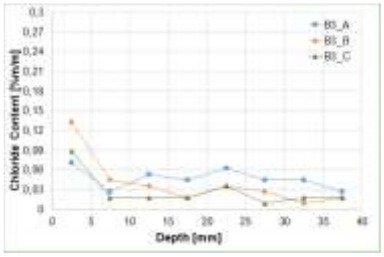

Initial crack width=123.5µm

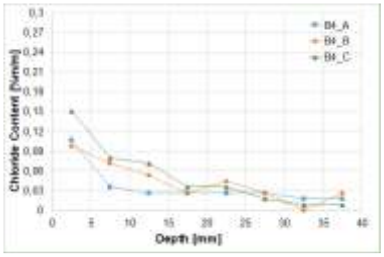

Uncracked

3 months

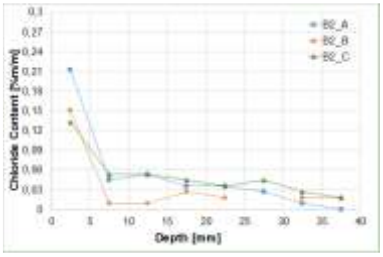

Initial crack width=85.3µm

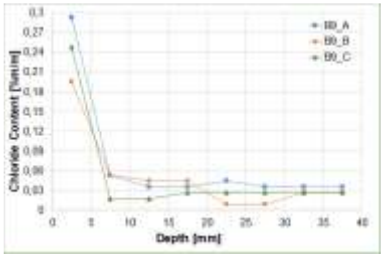

Initial crack width=84.8µm

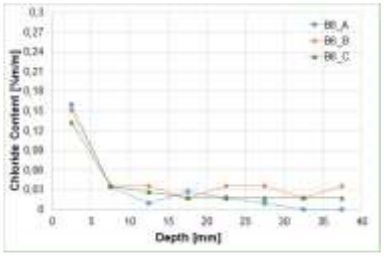

Uncracked

6 months

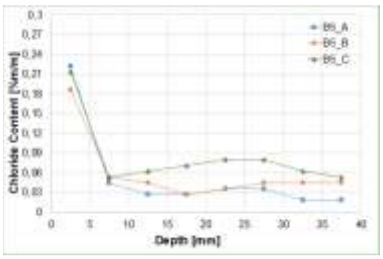

Initial crack width=150.6µm

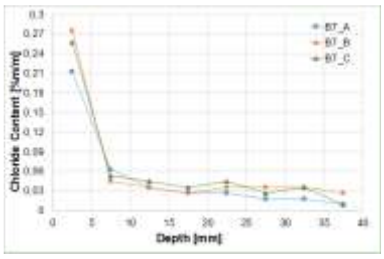

Initial crack width=58.6µm

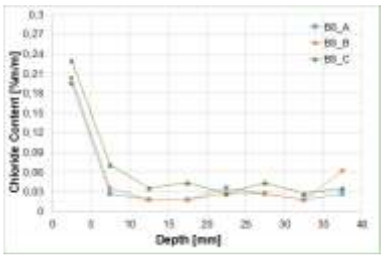

Uncracked

Figure 28. Chloride content vs. depth after 1, 3 and 6 months healing

From the chloride penetration profiles (Figure 28), the chloride apparent diffusion coefficient D_{app} was determined for uncracked and cracked specimens for the three healing periods studied (1, 3 and 6 months) and for all three positions analyzed with respect to the crack for cracked specimens (Figure 10). The D_{app} values are summarized in Table 10. The D_{app} values do not depend significantly on the position, whereas they are more affected by the duration of the healing period. In fact, D_{app} decreased drastically after 6 months healing compared to 1 month healing. This result was also observed by this research group for specimens of the same mix without nanoadditions [17].

Moreover, in order to analyze the possible influence of the presence of crystalline admixtures and CNFs, D_{app} were calculated for the following three mixes: UHPC, UHPC with crystalline admixtures and UHPC with crystalline admixtures and CNFs at different healing times (1, 3

and 6 months). The values without CNFs were obtained from a previous research [17]. The results are shown in Table 11. There were not significant differences regarding D_{app} values between the three mixes, only D_{app} values were slightly higher for the mix with CNFs but probably due to the higher initial crack width of this mix.

Table 10. Apparent chloride diffusion coefficients Dapp (10^{-12} m^2/s) of uncracked and cracked specimens with CNFs after 1, 3 and 6 months healing

			D_{app} [10^{-12} m^2/s]		
Healing time	**Specimen ID**	**Cracking**	**Position A**	**Position B**	**Position C**
1 month	B1	Cracked (w=86.9µm)	29.43	28.51	29.24
	B3	Cracked (w=123.5µm)	29.45	28.98	28.54
	B4	Uncracked	29.34	29.56	29.43
3 months	B2	Cracked (w=85.3µm)	6.69	9.38	19.63
	B9	Cracked (w=84.8µm)	9.06	8.56	8.68
	B6	Uncracked	4.73	10.90	8.67
6 months	B5	Cracked (w=150.6µm)	4.44	4.64	4.93
	B7	Cracked (w=58.6µm)	4.49	4.62	4.64
	B8	Uncracked	4.45	4.55	4.51

Table 11. Apparent chloride diffusion coefficients Dapp (10^{-12} m^2/s) for UHPC, UHPC with crystalline admixtures and UHPC with crystalline admixtures and CNFs at different healing times (1, 3 and 6 months)

D_{app} [10^{-12} m^2/s]	**UHPC**			**UHPC + crystalline admixtures**			**UHPC + crystalline admixtures + CNFs**		
Crack width ranges [µm]	25-100			20-100 (and two cases: 150 and 190 µm)			58-150		
Healing time	**A**	**B**	**C**	**A**	**B**	**C**	**A**	**B**	**C**
1 month	21.90	22.30	20.30	23.00	26.00	22.40	29.41	29.02	29.07
3 months	5.15	3.45	4.01	5.06	5.87	5.10	6.83	9.61	12.33
6 months	1.55	1.83	1.90	1.85	2.06	1.97	4.46	4.60	4.69

3.2. Microstructural analysis

To analyze the effects of the presence of CNFs in the UHPC matrix, Termogravimetry (TG), Derivative thermogravimetry (DTG) and Differential Thermal Analysis (DTA) were carried out on the concrete under study, UHPFRC+CNF, and on a reference one (same UHPFRC but without nanoadditions). TG (Figure 29a, Figure 29c) shows the weight loss (%) with respect to temperature (in ºC) for the UHPC+CNF and the reference one, UHPC, for both curing conditions, moist room and immersion in geothermal water. More relevant information can be

obtained from DTG curves where the peaks of C-S-H and gypsum (around 100 ºC), portlandite (around 400 ºC) and carbonate phases, $CaCO_3$ (around 600-700 ºC) can be clearly observed, although no significant differences were observed regarding the presence or absence of CNFs. From DTA curves (Figure 29b, Figure 29d), the changes on UHPC and UHPC+CNF can be observed. Both samples and the inert sample were subjected to temperature (heating program). No exothermic peaks were detected from DTA curves. On the contrary, all the peaks corresponded to endothermic reactions which match with weight losses in the corresponding TG curves. Specifically, around 100 ºC can be detected a strong endotherm related to water evaporation, whereas the endotherm at 400 ºC corresponds to the decomposition of hydroxides, at 700 ºC decomposition of carbonates and at 1200 ºC decomposition of sulphates.

X-ray diffraction patterns of UHPC+CNF and the reference one without nanoadditions (UHPFRC) are reported in Figure 30. No substantial differences were observed in presence of CNFs. As expected, for both analyzed mixes (with and without CNFs) the usual concrete composites such as quartz, ettringite, calcite portlandite, albite were observed. No relevant influence was observed neither due to the curing condition (moist room or immersion in geothermal water) nor to the presence of CNFs. The diffraction peaks of portlandite at 18º, 34.3º and 47º and ettringite (E) were similar for both types of concrete and both types of curing condition. Only diffraction peaks slightly higher of ettringite (24.7º) and hatrurite (29.5º) were observed for specimens cured in moist room no matter the presence or absence of CNFs. Moreover the diffraction peak of zeolite (12º) was lower when specimens were immersed in geothermal water.

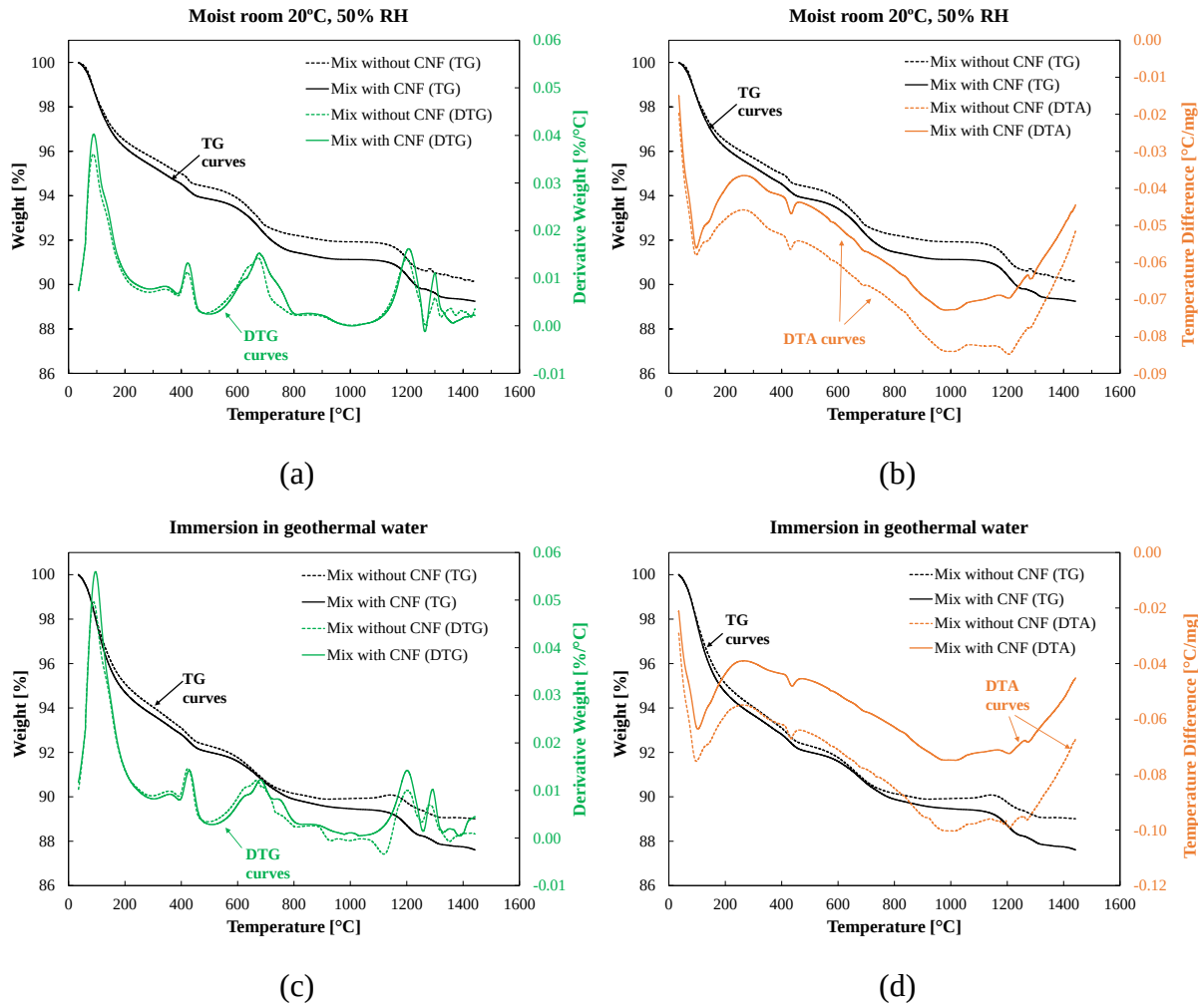

Figure 29. TG, DTG and DTA curves of UHPFRC and UHPFRC+CNF cured in moist room and immersed in geothermal water.

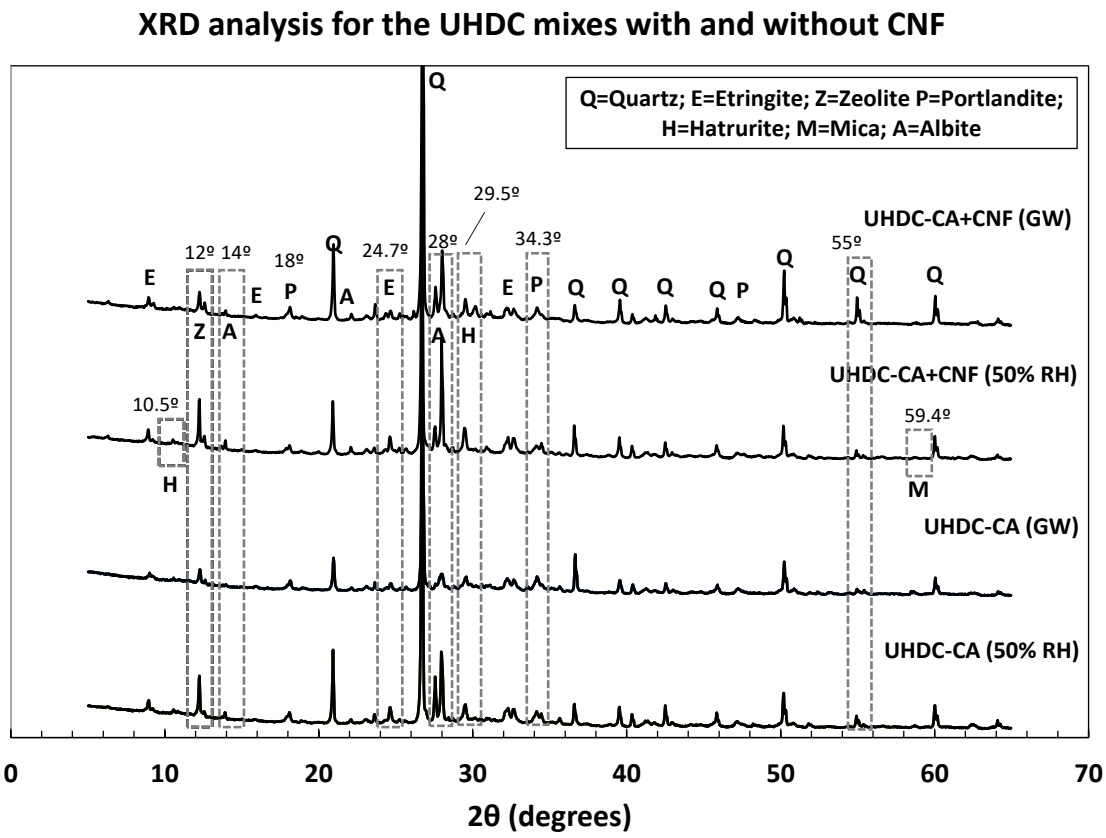

Figure 30. XRD analysis of UHPFRC and UHPFRC+CNF cured in moist room and immersed in geothermal water.

4. CONCLUSIONS

In this paper, the influence of crack healing on the recovery of durability (water permeability tests and chloride diffusion tests) and mechanical properties (flexural strength and stiffness) of Ultra High Performance Concretes (UHPC) with cellulose nanofibers (CNF) has been analyzed. To this purpose, the recovery of the properties was quantified by means of suitably defined indexes: Index of Crack Sealing, Index of Permeability Healing, Index of Stress Capacity Recovery and Index of Stiffness/Damage Recovery. A comparison was also performed with the reference mix, without nanoadditions, as well as with a companion mix obtained from the same reference one but with alumina nanofibers, both from previous experimental campaigns from the same research group.

From the analysis of the results, the following conclusions can be drawn regarding the mix with cellulose nanofibers:

- The presence of cellulose nanofibers (CNFs) has improved the crack self-sealing. For a same healing period (1, 3 and 6 months) the specimens with CNFs reached higher Index of

Crack Sealing (ICS) values than those without CNFs. This improvement is due to the fact that CNFs carries water and stimulates reactions, thanks to its specific surface 100 times higher than the one of cement and slag.

- Crack sealing was better for specimens immersed in geothermal water compared to those cured in moist room, surely due to the larger and continuous supply of water and no matter the presence, in the geothermal water, of aggressive ions. With this conditions CNFs promote internal curing and hence improving self-sealing. As a matter of fact, for same range of initial crack width (4-40μm) the Index of Crack Sealing (ICS) ranged from 30 to 93% for specimens immersed in geothermal water whereas it ranged from 14 to 80% in specimens cured in moist room. Moreover, after 1 month of healing the average value of ICS or specimens immersed in geothermal water was twice as much the one of specimens cured in moist room with ICS values of 60 and 30% respectively.
- After three re-cracking and healing cycles (1+2+3 months) the ICS values were similar for both studied conditions, moist room and geothermal water. Moreover, the cracking-healing cycles affected the crack sealing since the crack was reopened for several times and being progressively decreasing the amount of unhydrated cement particles and hence diminishing the sealing capacity. Nevertheless, after three healing-cracking cycles, the UHPFRC+CNFs keeps a certain crack sealing capacity generally higher than after the first cracking-healing cycle, surely due to the combination of several effects: the UHPFRC has numerous unhydrated cement particles, the long-term benefits on self-healing due to the addition of crystalline admixtures and the internal curing role played by CNFs. On the other hand, when specimens were pre-cracked and then were continuously immersed in geothermal water (without intermediate re-cracking), the ICS value increased continuously with the duration of healing exposure. The general trend has confirmed that the wider the crack width, the lower the crack sealing. Moreover, specimens with CNFs reached higher Index of Crack Sealing (ICS) for a same crack width value. This confirms the role of CNFs as promoters of internal curing improving the self-sealing capacity.
- The Index of Strength Recovery (ISR) decreased with the crack width. The highest ISR values were reached by the specimens immersed in geothermal water. Anyway, no significant improvements were observed when CNFs were present. On the contrary, the higher ISR values were observed when alumina nanofibers (ANFs) were included in the mix, always in comparison with the reference mix containing no additions, which proves the effect of ANFs toughening the concrete matrix, and hence improving the self-healing

behavior.

- Both mechanical recovery indices, ISR and Index of stiffness/Damage Recovery (IDaR) were directly proportional to ICS. High values of ISR and IDaR corresponded to high values of ICS.
- The Index of Permeability Healing (IPH) reached a 100% when the cracks were completely healed after 6 months. IPH was inversely proportional to crack width since when the crack width increased, the IPH decreased. Moreover, the ICS and IPH were directly proportional since when ICS increased, the IPH also increased. The longer the healing time, the higher the value of both indices. The presence of CNFs increased the IPH value for a same ICS compared to the mix without nanoadditions.
- Regarding the specimens with CNFs, for crack widths lower than 120μm immersed in geothermal water for 3 and 6 months the chloride content was very similar to the uncracked specimens since the cracks were sealed.
- The apparent chloride diffusion coefficients (D_{app}) did not depend significantly on the position with respect to the crack, they depended more on the duration of the healing period. As a matter of fact, D_{app} sharply diminished after 6 months healing compared to 1 month healing.

ACKNOWLEDGMENTS

The research activity reported in this paper has been performed in the framework of the ReSHEALience project (Rethinking coastal defence and Green-energy Service infrastructures through enHancEd-durAbiLity high-performance cement-based materials) which has received funding from the European Union's Horizon 2020 research and innovation program under grant agreement No 760824. The information and views set out in this publication do not necessarily reflect the official opinion of the European Commission.

The kind collaboration of the ReSHEALience partners API-Europe and Penetron Italia are acknowledged, in supplying respectively cellulose nanofibers and the crystalline admixtures. Kind help of ReSHEALience partner EGP in allowing visits to geothermal plants in Tuscany for geothermal water supply is also acknowledged. The authors also thank BuzziUnicem, Azichem Ltd. and BASF Italia for supplying of cement, steel fibers and superplasticizer respectively, employed for casting the different investigated UHDC mixes.

The help of Mr. Antonio Cocco and Mr. Paolo Broglia (Laboratory for Testing Materials, Buildings and Structures, Politecnico di Milano) in casting specimens for the experimental

programme and providing organizational support for its execution is gratefully acknowledged.

REFERENCES

[1] WorldEconomicForum, "Shaping the Future of Construction. A Breakthrough in Mindset and Technology. Prepared in collaboration with The Boston Consulting Group," 2016.

[2] E. Gomez, B. LeporaceGuimil, A. Conforti, G. Plizzari, G. Duffo and R. Zerbino, "A practical approach for monitoring reinforcement corrosion in steel fiber reinforced concrete elements exposed to chloride rich environments," *Structural Journal*, pp. 1-14, 2022.

[3] B. LeporaceGuimil, A. Conforti, R. Zerbino and G. Plizzari, "Chloride-induced corrosion in reinforced concrete and fiber reinforced concrete elements under tensile service loads," *Cement and Concrete Composites,* vol. 124, p. 104245, 2021.

[4] S. Mattews, "CONREPNET: Performance-based approach to the remediation of reinforced concrete structures: Achieving durable repaired concrete structures," *Journal of Building Appraisal,* vol. 3, no. 1, pp. 6-20, 2007.

[5] E. Cuenca, M. Criado, M. Giménez, M. Alonso and L. Ferrara, "Effects of alumina nanofibers and cellulose nanocrystals on durability and self-healing capacity of ultra-high performance fiber reinforced concretes (UHPFRC)," *Journal of Materials in Civil Engineering,* vol. 34, no. 8, 2022.

[6] W. Wang, J. Liu, F. Agostini, C. Davy, F. Skoczylas and D. Corvez, "Durability of an ultra high performance fiber reinforced concrete (UHPFRC) under progressive aging," *Cement and Concrete Research,* vol. 55, pp. 1-13, 2014.

[7] C. Shi, Z. Wu, J. Xiao, D. Wang, Z. Huang and Z. Fang, "A review on ultra high performance concrete: Part I. Raw materials and mixture design," *Construction and Building Materials,* vol. 101, pp. 741-751, 2015.

[8] C. Alonso, C. Andrade, E. Menéndez and E. Gayo, "Microstructural changes in high and ultra high strength concrete exposed to high temperature environments," *ACI Special Pubblication,* vol. 229, pp. 289-302, 2005.

[9] K. Li and L. Li, "Crack-altered durability properties and performance of structural concretes," *Cement and Concrete Research,* vol. 124, p. 105811, 2019.

[10] E. Cuenca, L. DAmbrosio, D. Lizunov, A. Tretjakov, O. Volobujeva and L. Ferrara, "Mechanical properties and self-healing capacity of Ultra High Performance Fibre Reinforced Concrete with alumina nano-fibres: Tailoring Ultra High Durability Concrete for aggressive exposure scenarios," *Cement and Concrete Composites,* vol. 118, p. 103956, 2021.

[11] E. Cuenca, S. Rigamonti, E. Gastaldo and L. Ferrara, "Crystalline admixture as healing promoter in concrete exposed to chloride-rich environments: experimental study," *Journal of Materials in Civil Engineering,* vol. 33, no. 3, p. 04020491, 2021.

[12] D. DiSumma, J. TenorioFilho, D. Snoeck, P. VandenHeede, S. VanVierberghe, L. Ferrara and N. DeBelie, "Environmental and economic sustainability of crack mitigation in reinforced concrete with SuperAbsorbent Polymers (SAPs)," *Journal of Cleaner Production,* vol. 336, p. 130213, 2022.

[13] J. Lopez, P. Serna, J. NavarroGregori and H. Coll, "A simplified five-point inverse analysis method to determine the tensile properties of UHPFRC from unnotched four-point bending tests," *Composites Part B: Engineering,* vol. 91, pp. 189-204, 2016.

[14] K. Sisomphon, O. Copuroglu and E. Koenders, "Self-healing of surface cracks in mortars with expansive additive and crystalline additive," *Cement and Concrete Composites,* vol. 34, no. 4, pp. 566-574, 2012.

[15] A. DeSouzaOliveira, O. daFonsecaMartinsGomez, L. Ferrara, E. deMoraesRegoFairbairn and R. ToledoFilho, "An overview of a twofold effect of crystalline admixtures: From permeability-reducers to self-healing stimulators," *Journal of Building Engineering,* vol. 41, no. 102400, pp. 1-20, 2021.

[16] E. Cuenca, A. Mezzena and L. Ferrara, "Synergy between crystalline admixtures and nano-constituents in enhancing autogenous healing capacity of cementitious composites under cracking and healing cycles in aggressive waters," *Construction and Building Materials,* vol. 266, p. 121447, 2021.

[17] E. Cuenca, F. LoMonte, M. Moro, A. Schiona and L. Ferrara, "Effects of Autogenous and Stimulated Self-Healing on Durability and Mechanical Performance of UHPFRC: Validation of Tailored Test Method through Multi-Performance Healing-Induced Recovery Indices," *Sustainability,* vol. 13, p. 11386, 2021.

[18] F. LoMonte and L. Ferrara, "Tensile Behaviour Identification in Ultra-High Performance Fibre Reinforced Cementitious Composites: Indirect Tension Tests and Back Analysis of Flexural Test Results," *Materials and Structures,* vol. 53, no. 145, pp. 1-12, 2020.

[19] Z. Wu, C. Shi, K. Khayat and S. Wan, "Effects of different nano-materials on hardening and performance of ultra-high strength concrete (UHSC)," *Cement and Concrete Composites,* vol. 70, pp. 24-34, 2016.

[20] K. Sobolev, "Modern developments related to nanotechnology and nanoengineering of concrete," *Front. Struct. Civ. Eng.*, vol. 10, no. 2, pp. 131-141, 2016.

[21] R. Gopalakrishnan and R. Jeyalakshmi, "Strength deterioration of nano-silica contained in ordinary Portland cement concretes in aggressive sulfate environments," *Eur. Phys. J. Plus,* vol. 133, no. 351, pp. 1-19, 2018.

[22] M. KonstaGdoutos, G. Batis, P. Danoglidis and E. Zacharopoulou, "Effect of CNT and CNF loading and count on the corrosion resistance, conductivity and mechanical properties of nanomodified OPC mortars," *Construction and Building Materials,* vol. 147, pp. 48-57, 2017.

[23] A. Materazzi, F. Ubertini and A. DAlessandro, "Carbon nanotube cement-based transducers for dynamic sensing of strain," *Cement and Concrete Composites,* vol. 37, pp. 2-11, 2013.

[24] A. DAlessandro, M. Rallini, F. Ubertini, A. Materazzi and J. Kenny, "Investigations on scalable fabrication procedures for self-sensing carbon nanotube cement-matrix composites for SHM applications," *Cement and Concrete Composites,* vol. 65, pp. 200-213, 2014.

[25] E. Deze, E. Cuenca, M. Nasner, S. Iakovlev, S. Sideri, A. Sapalidis, R. Borg and L. Ferrara, "Nanocellulose enriched concretes: evaluation of nano-cellulose properties

affecting durability and development of mixing protocols," *Materials Today Proceedings,* vol. 54, no. 1, pp. 50-56, 2022.

[26] O. Hisseine, W. Wilson, L. Sorelli, B. Tolnai and A. TagnitHamou, "Nanocellulose for improved concrete performance: A macro-to-micro investigation for disclosing the effects of cellulose filaments on strength of cement systems," *Construction and Building Materials,* vol. 206, pp. 84-96, 2019.

[27] L. Jiao, M. Su, L. Chen, Y. Wang, H. Zhu and H. Dai, "Natural Cellulose Nanofibers As Sustainable Enhancers in Construction Cement," *PLos One,* vol. 11, no. 12, p. e0168422, 2016.

[28] V. Kokol, M. Bozic, R. Vogrincic and A. Mathew, "Characterisation and properties of homo- and heterogenously phosphorylated nanocellulose," *Carbohydrate Polymers,* vol. 125, pp. 301-313, 2015.

[29] D. Trache, A. Tarchoun, M. Derradji, O. Mehelli, M. Hussin and W. Bessa, "Cellulose fibers and nanocrystals: preparation, characterization and surface modification," in *Functionalized Nanomaterials I: Fabrication*, CRC Press, 2020.

[30] R. Moon, G. Schueneman and J. Simonsen, "Overview of cellulose nanomaterials, their capabilities and applications," *The Journal of The Minerals, Metals & Materials Society (JOM),* vol. 68, pp. 2383-2394, 2016.

[31] R. Moon, A. Martini, J. Nairn, J. Simonsen and J. Youngblood, "Cellulose nanomaterials review: Structure, properties and nanocomposites," *Chemical Society Reviews Journal,* vol. 40, no. 7, pp. 3941-3994, 2011.

[32] O. Onuaguluchi, D. Panesal and M. Sain, "Properties of nanofibre reinforced cement composites," *Construction and Building Materials,* vol. 63, pp. 119-124, 2014.

[33] T. Fu, F. Montes, P. Suraneni, J. Youngblood and J. Weiss, "The Influence of Cellulose Nanocrystals on the Hydration and Flexural Strength of Portland Cement Pastes," *Polymers,* vol. 9, no. 9, p. 424, 2017.

[34] Y. Cao, P. Zavattieri, J. Youngblood, R. Moon y J. Weiss, «The influence of cellulose nanocrystal additions on the performance of cement paste,» *Cement and Concrete Composites,* vol. 56, pp. 73-83, 2015.

[35] M. Ardanuy, J. Claramunt, R. Arevalo, F. Pares, E. Aracri and T. Vidal, "Nanofibrillated cellulose (NFC) as a potential reinforcement for high performance cement mortar composites," *BioResources,* vol. 7, no. 3, pp. 3883-3894, 2012.

[36] Y. Cao, P. Zavattieri, J. Youngblood, R. Moon and J. Weiss, "The relationship between cellulose nanocrystal dispersion and strength," *Construction and Building Materials,* vol. 119, pp. 71-79, 2016.

[37] O. Onuaguluchi and N. Banthia, "Plant-based natural fibre reinforced cement composites: A review," *Cement and Concrete Composites,* vol. 68, pp. 96-108, 2016.

[38] R. Mejdoub, H. Hammi, J. Suñol, M. Khitouni, A. Mnif and S. Boufi, "Nanofibrillated cellulose as nanoreinforcement in Portland cement: Thermal, mechanical and microstructural properties," *Journal of Composite Materials,* vol. 51, no. 17, pp. 2491-2503, 2017.

[39] T. DaCunhaMoreira, V. Krelani, S. Ferreira, L. Ferrara and R. ToledoFilho, "Self-healing of slag cement Ultra High Performance Steel Fiber Reinforced Concrete (UHPFRC) containing sisal fibers as healing conveyor," *Journal of Building Engineering,* vol. 54, p. 104638, 2022.

[40] X. Sun, Q. Wu, S. Lee, Y. Qing and Y. Wu, "Cellulose nanofibers as a modifier for rheology, curing and mechanical performance of oil well cement," *Nature Scientific Reports,* vol. 6, p. 31654, 2016.

[41] S. AlObaidi, P. Bamonte, F. Animato, F. Lo Monte, I. Mazzantini, M. Luchini, S. Scalari and L. Ferrara, "Innovative Design Concept of Cooling Water Tanks/Basins in Geothermal Power Plants using Ultra High Performance Fiber Reinforced Concrete with Enhanced Durability," *MPDI Sustainability,* vol. 13, no. 17, pp. 1-26, 2021.

[42] S. AlObaidi, P. Bamonte, M. Luchini, I. Mazzantini and L. Ferrara, "Durability-based design of structures made with UHP/UHDC in extremely aggressive scenarios:

application to a geothermal water basin case study," *MDPI Infrastructures*, vol. 5, no. 11, pp. 1-44, 2020.

[43] S. AlObaidi, M. Davolio, F. LoMonte, P. Bamonte and L. Ferrara, "Structural validation of geothermal water basins constructed with durability enhanced ultra high performance fibre reinforced concrete (Ultra High Durability Concrete)," *Case Studies in Construction Materials*, vol. 17, p. 01202, 2022.

[44] E. Cuenca, A. Tejedor and L. Ferrara, "A methodology to assess crack-sealing effectiveness of crystalline admixtures under repeated cracking-healing cycles," *Construction and Building Materials*, vol. 179, pp. 619-632, 2018.

[45] L. Ferrara, V. Krelani and M. Carsana, "A "fracture testing" based approach to assess crack healing of concrete with and without crystalline admixtures," *Construction and Building Materials*, vol. 68, pp. 535-551, 2014.

[46] M. DiPrisco, L. Ferrara and G. Lamperti, "Double edge wedge splitting (DEWS): An indirect tension test to identify post-cracking behaviour of fibre reinforced cementitious composites," *Materials and Structures*, vol. 46, no. 11, pp. 1893-1918, 2013.

[47] C. Litina, G. Bumanis, G. Anglani, M. Dudek, R. Maddalena, M. Amenta, S. Papaioannou, G. Perez, J. GarciaCalvo, E. Asensio, R. BeltránCobos, F. TavaresPinto, A. Augonis, R. Davies, A. Guerrero, M. SanchezMoreno, T. Stryszewska, I. Karatasious and e. al, "Evaluation of Methodologies for Assessing Self-Healing Performance of Concrete with Mineral Expansive Agents:An Interlaboratory Study," *Materials*, vol. 14, no. 2024, pp. 1-26, 2021.

1

2